# EXPERIMENTAL STUDY OF ALUMINA-WATER AND ZIRCONIA-WATER NANOFLUIDS CONVECTIVE HEAT TRANSFER AND VISCOUS PRESSURE LOSS IN LAMINAR REGIME

By

Ulzie L. Rea

SUBMITTED TO THE DEPARTMENT OF MECHANICAL SCIENCE
AND ENGINEERING
IN PARTIAL FULFILLMENT OF THE REQUIREMENTS FOR THE DEGREE OF

BACHELOR OF SCIENCE IN MECHANICAL ENGINEERING
AT THE
MASSACHUSETTS INSTITUTE OF TECHNOLOGY

JANUARY 2008
[February 2008]



Signature of Author: _____
Department of Mechanical Engineering
January 18th 2008

Certified by _____
Lin-Wen Hu, Thesis Supervisor
Associate Director, Nuclear Reactor Laboratory

_____
Jacopo Buongiorno, Thesis Co-supervisor
Assistant Professor of Nuclear Science and Engineering

_____
Tom McKrell, Thesis Reader
Research Scientist of Nuclear Science and Engineering Department

Accepted by: _____
John H. Lienhard V
Professor of Mechanical Engineering
Chairman, Undergraduate Thesis Committee

# EXPERIMENTAL STUDY OF ALUMINA-WATER AND ZIRCONIA-WATER NANOFLUIDS CONVECTIVE HEAT TRANSFER AND VISCOUS PRESS URE LOSS IN LAMINAR REGIME

By

Ulzie L. Rea

Submitted to the Department of Mechanical Engineering on January 18th 2008
In Partial Fulfillment of the Requirements for the Degree of
Bachelor of Science in Mechanical Engineering

## ABSTRACT

The objective of this study is to evaluate experimentally the convective heat transfer and viscous pressure loss characteristics of alumina-water and zirconia-water nanofluids. Nanofluids are colloidal dispersions of nanoparticles in metal, metal oxide, carbon-based materials in base fluids, and may offer improved heat transfer properties compared with pure base fluids. A flow loop with a vertical heated section was designed and constructed to operate in the laminar flow regime (Re<2000). Initial tests were conducted with de-ionized water for experiment validation. Alumina nanofluid was tested in the flow loop at four different volumetric loadings, 0.6%, 1%, 3% and 6% and zirconia nanofluid was tested at volumetric loadings of 0.3%, 0.64% and 1.3%. The experimental results, represented in Nusselt number (Nu) and dimensionless length $x^+$, are in good agreement with traditional model predictions if the loading- and temperature- dependent thermophysical properties are utilized. Measured pressure loss of the nanofluid is within 20% of theory. It is concluded that the laminar convective heat transfer and viscous pressure loss behavior of alumina-water and zirconia-water nanofluids can be predicted by existing models as long as the correct mixture properties are used, and there is no abnormal heat transfer enhancement.

Thesis Supervisor: Lin-Wen Hu
Title: Associate Director and Principal Research Scientist
MIT Nuclear Reactor Laboratory

Thesis Supervisor: Jacopo Buongiorno
Title: Assistant Professor
MIT Nuclear Science and Engineering Department

## ACKNOWLEDGEMENT

I would like to take this time to thank the following people, who were vital to the completion of this thesis. I would like to thank my Dad, Mom, Sister, Grandma, Aunt Inez, and Uncle John for their support both mentally and financially during my education endeavor. Further, I am appreciative of Professor Jacopo Buongiorno's advice and aid given throughout the project. I want to thank Dr. Wesley Williams and Dr. Tom McKrell for their help and guidance in construction of the experimental facility; as well as Darryl Walton and Dr. Gordon Kohse for their help with characterization of nanofluids. I am appreciative for the patience, support, and direction of Dr. Lin-Wen Hu. She gave me the opportunity to work on this experiment and supervised the completion of this work. I am grateful and blessed to have the people above teach me a valuable lesson and experience about not only research, but life in general.

**TABLE OF CONTENTS**

**LIST OF TABLES**

Table No. Page

**LIST OF FIGURES**

Figure No. Page

**LIST OF SYMBOLS**

| Symbol | Definition |
|---|---|
| Nu | Nusselt Number |
| H | Heat transfer coefficient [J/kg] |
| D | Diameter [m] |
| K | Thermal Conductivity [W/(m*k)] |
| $D_B$ | Brownian diffusion coefficient |
| $k_B$ | Boltzmann's constant [J/K] |
| T | Temperature [K] |
| Re | Reynolds number |
| V | Velocity [m/s] |
| R | Radius [m] |
| $c_p$ | Specific Heat Capacity [J/(kg*K)] |
| Pr | Prandtl Number |
| $f_f$ | Friction factor |
| $X^+$ | Dimensionless axial location |
| L | Length [m] |
| I | Current [A] |
| V | Voltage [V] |
| $\dot{m}^*$ | Mass flow rate [kg/s] |
| Greek Letters | |
| $\mu$ | Viscosity [Pa*s] |
| $\rho$ | Density [kg/ $m^3$] |
| $\alpha$ | Thermal Diffusivity [$m^2$/s] |
| $\Delta$ | Difference |
| Subscripts | |
| P | Nanoparticles |
| $F$ | Fluid |
| Sol | Particle solid |

| | |
|---|---|
| Elec | Electrical |
| Therm | Thermal |

# CHAPTER 1

# INTRODUCTION

## 1.01 THESIS OBJECTIVE

The objective of this thesis is to study whether nanofluids are able to provide advantages in heat transfer applications over their pure liquid counterparts. Furthermore the focus of this study is to measure the heat transfer coefficient and viscous pressure loss in the laminar flow regime. The following questions are addressed in this research: will nanofluids be able to increase the thermal conductivity of base fluids? will nanofluids prove to be useful in increasing heat transfer coefficient? and ultimately will water-based nanofluids be better fluids in the laminar flow domain? These are some of the questions that researchers are striving to answer. The goal of this research is to obtain experimental data by utilizing an experimental loop through which heat transfer rate and pressure drop are measured. Two types of nanofluids are tested in this study – alumina-water and zirconia-water nanofluids. Experimental results of these nanofluids are compared with theory/correlation to evaluate whether they offer advantages over pure fluid.

## 1.1 BACKGROUND

In order to understand the characteristics of nanofluids, a review of some previous work in this area is given below.

### 1.1.1 Thermal Conductivity

For the purpose of heat transfer, thermal conductivity is an important parameter. The thermal conductivity of common fluids is low compared to that of solids, such as metals or metal oxides. Nanofluid is an innovative approach to create higher thermal

conductivity to meet the demand in high power thermal management systems. There have been earlier attempts to place micron-sized solid particles in liquids, but problems have occurred with particles settling. The nano-scale particles are small enough to form a stable dispersion in the liquid.

### 1.1.2 Model for Heat Enhancement of Nanofluids

Theoretically, the thermal conductivity increases are based on the volume fraction and shape of the particles. The Argonne National Laboratory [1] performed nanofluid experiments, where it was found there was a 20% increase in thermal conductivity. This was found true with base fluid ethylene glycol and copper oxide particles with volume percent of 4. It was shown that there is a strong correlation between volume percent and thermal conductivity enhancement.

The increase of thermal conductivity leads to an increase in heat transfer performance. The Nusselt number (Nu) is a dimensionless number that represents the ratio between convective and conductive heat transfer. It is defined as:

$$Nu = \frac{h * D_{inner}}{k} \tag{1.1}$$

where h is the heat transfer coefficient, $D_{inner}$ is the inner diameter of the pipe, and k is the thermal conductivity of the fluid. If the thermal conductivity increases, then the heat transfer coefficient will increase in theory, provided Nu is constant. According to the theory the Nusselt number should remain constant at 4.36 in the fully-developed laminar region where the Reynolds number is below 2100. There have been experiments from the Argonne National Laboratory [1], where testing was done with Alumina. Their results yielded heat transfer improvements of 80% with a volume percent of less than 3.

### 1.1.3 Colloids

Nanofluids are engineered colloids. A colloid is a homogeneous mixture that consists of two different phases: dispersed-phase particles normally between 1 to 100 nm and a continuous liquid phase.

One problem that has occurred in the past is to keep the solid particles from aggregating. The agglomeration of particles can be prevented by using surfactants or by tuning the surface charge of the particles. The surfactant molecules can best be represented as having a hydrophobic head, which is a particle that repels water and hydrophilic tail which is attracted to water. The hard component of keeping the colloid stable has to do with the particle's being repulsive to the base fluid and holding an attractive charge [2]. This feature in colloids leads to colloids aggregating upon collision. This is usually prevented by giving the particles similar charges and thus repelling one particle from another.

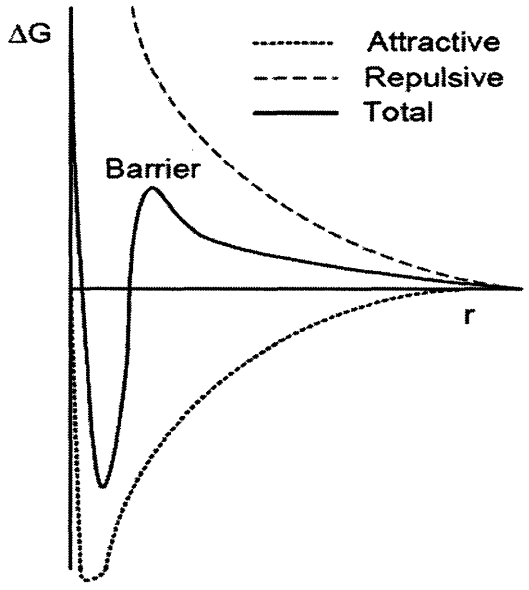


**Figure 1.1: This shows the energy that is required to surmount the inter-particle forces (Adopted from [6])**

From the graph it can be seen that the energy it takes to overcome two repulsive forces as they come closer is high. Once this energy barrier is exceeded then the particles agglomerate, which may mean that the particles become heavier than the base fluid and sedimentation occurs. This would make it difficult for Brownian Motion to keep the particles in suspension.

### 1.1.4 Brownian Motion

It has been theorized that the basis around colloid stability revolves around Brownian motion. Brownian motion is defined as the random movement of particles in a base fluid. This random movement means that there is a collision of particles into one another. The particles impact upon other particles is negligible because the concentration of particles in nanofluids is normally low. The particles impact to molecules is important. This collision passes on the kinetic energy of the previous particle obtained to the molecules. Brownian motion has been researched by Jang and Choi [3] to give off energy more effectively from the random motion of nanoparticles rather than the collision of nanoparticles. They explain that conduction is able to occur due to the interaction that nanoparticles and liquid molecules have. Brownian motion is best described mathematically from the Einstein-Stokes's equation:

$$D_B = \frac{k_B T}{3\pi * \mu * d_p} \tag{1.2}$$

In this equation $D_B$ represents the Brownian diffusion coefficient, $k_B$ Boltzmann's constant, $\mu$ viscosity, and $d_p$ is the diameter of the nanoparticle.

## 1.2 RECENT WORK IN NANOFLUID CONVECTIVE HEAT TRANSFER

There have been important studies in the area that will be discussed in this section. The work of Kwak and Kim [4] refers to heat transfer enhancement and nanofluids were found to be more efficient if the nanoparticles are spherical in shape. Xuang and Li [5] investigated the effects of nanofluids in turbulent flow. In their experiment, copper nanoparticles were used. Their research found increases in heat transfer coefficients in the copper nanofluids compared to water at similar Reynolds numbers. The overall result of this research presents heat enhancement increases as volume fraction of the nanofluid rises. Williams [6] at MIT studied heat transfer convection of nanofluids in the turbulent domain. His work included investigations of alumina and zirconia nanofluids. This research found that there was no heat transfer enhancement from the nanofluids in turbulent flow region. It was discovered that the comparison of heat transfer coefficient and Reynolds number, a dimensionless number, with that of nanofluids and water was a wrong approach to take. Prandtl number also attributed to heat transfer coefficient increase because of the large difference of viscosity between de-ionized water and the nanofluids.

Work has also been done in the laminar flow domain by Wen and Ding [7]. They investigated the heat transfer of nanofluids under laminar flow and focused on the entrance region. Their research used alumina nanofluids and concluded that heat transfer enhancement increases with particle concentration and Reynolds numbers. In particular, they noticed that there was an increase in heat transfer capability at the entrance region of the pipe and then steady decline with increased distance. They hypothesized that thermal conductivity of nanofluid is not the main cause for heat transfer enhancement, but rather

it is possibly due to particle migration which results in non-uniform distribution of thermal conductivity and viscosity field which reduces the thermal boundary layer thickness.

Buongiorno [9] offers reasons for the nanofluids convective heat transport in the turbulent regime. He proposes that there are seven slip mechanisms used to determine such behavior and they are inertia, Brownian Diffusion, Thermophoresis, Diffusiophoresis, Magnus Effect, Fluid Drainage, and Gravity. He further clarifies that the two most important of these features are Thermophoresis, where particles disperse caused by a temperature gradient, and Brownian Diffusion, which is the random collision and movement of particles suspended in a base fluid. Buongiorno explains that heat transfer enhancement occurs when the viscosity is less and the laminar sublayer of the boundary layer is small.

Table 1.1: Findings in Convective Heat Transfer

| Reference # | Authors | Regimes | Findings |
|---|---|---|---|
| 4 | Kwak and Kim | N/A | - Heat Enhancement more efficient when nanoparticles are spherical<br>- Rotational Brownian motion reduces enhancement due to geometry |
| 5 | Xuan and Li | Turbulent | - Increase in heat transfer coefficient using same Reynolds numbers of water and Cu nanofluids |
| 6 | W. Williams | Turbulent | - No heat transfer enhancement from turbulent flow<br>- Overlooked power it takes to pump the higher viscous fluids |

| | | | |
|---|---|---|---|
| 7 | Wen and Ding | Laminar | - Heat transfer enhancement found near the entrance region<br>- Enhancement can be attributed to the reduction of thermal boundary layer thickness. |
| 8 | A. Ahuja | N/A | - thermal conductivity is 3 times higher when moving opposed to stationary flow |
| 9 | J. Buongiorno | Turbulent | - There are seven slip mechanism to determine nanofluids behavior<br>- The two important ones are Thermophoresis and Brownian diffusion<br>- Enhancement occurs because the laminar sublayer is small |

# CHAPTER 2

# NANOFLUID PROPERTIES

## 2.1 NANOFLUID PROCUREMENT AND PREPARATION

There are various methods that are used to create nanofluids. In one process, the nanoparticles are made using gas condensation. The nanoparticles are then dispersed in the base fluid. Ultrasound is commonly used in this process in order to make sufficient amalgamation of base fluid and particle.[12] Another method called VEROS (Vacuum Evaporation on Running Oil Substrate) was used to prepare nanofluids by evaporating nanofluid particles on an oil substrate. A small metal particle is evaporated onto an oil substrate. The particles grew onto the oil substrate in the base fluid.

The nanofluids used in this experiment were purchased directly from the vendor NYACOL. They manufactured alumina and zirconia nanofluids with a nominal weight percent of 20 % as provided from the tables below [10].

Table 2.1: Alumina Nanofluid Properties from NYACOL:

| NAME | **NYACOL®<br>AL20DW** |
|---|---|
| $AL_2O_3$ (Wt. %) | 20 |
| Particle Size (nm) | 50 |
| Particle Charge | + |
| pH | 4.0 |
| Specific Gravity | 1.19 |
| Viscosity (cPs) | 10 |
| $AL_2O_3$ (Wt. %) | 20 |

Table 2.2: Zirconia Nanofluid Properties from NYACOL:

| NAME | **NYACOL®** **$ZrO_2$ (ACETATE STABILIZED)** |
|---|---|
| $ZrO_2$ (Wt. %) | 12.8% |
| Particle size, nm | 50 |
| Particle charge | + |
| Counter ion, mole/mole | 1.5 acetate |
| pH | 3.5 |
| Specific Gravity | 1.26 |
| Viscosity | 10 |

In the experiment, we wish to use diluted nanofluids at lower percents and the expression below was used to find the volume percent from a given weight percent"

$$\frac{Weight\% * \rho_f}{\rho_{sol} * (1 - Weight\%) + (Weight\% * \rho_f)} = Vol\% \tag{2.1}$$

The as-purchased weight percent is known; therefore, the volume % can be found by coming up with an arbitrary fraction of 20% alumina over water and alumina mixed. Knowing the $\rho_{sol}$, and $\rho_{AL}$, which is 3920 kg/m$^3$ for alumina, is important for finding the volume %. $\rho_{DI\&AL}$ is the mixed density of de-ionized water and alumina, which is found from the following equation [3],

$$\rho_{mix} = ((1 - Vol\%) * \rho_{liq}) + (Vol\% * \rho_{solid}) \tag{2.2}$$

For example, with 20 weight percent from equation (2) a $\rho_{DI\&AL}$ of 1584 kg/m$^3$ is found. From equation (1) a volume % of 6 is found. It is important to understand how

much needs to be added to a sample in order to experiment on the next set of volume or weight percent conditions. This is found from the following equation from [11]:

$$f = x\frac{\frac{1-DVol\%}{DVol\%} - \frac{1-Weight\%}{Weight\%} * \frac{\rho_f}{\rho_n}}{1+\frac{1-Weight\%}{Weight\%} * \frac{\rho_f}{\rho_n}} \tag{2.3}$$

In the above equation, $DVol\%$ is the desired volume % wanted, $\rho_f$ is the density of the base fluid, $\rho_n$ is the density of the nanopowder, x is the volume of the weight % being used, and $f$ represents the amount of the base fluid that is needed to dilute the fluid in order to obtain the desired volume %.

## 2.2 CHARACTERIZATION OF NANOFLUIDS

Nanoparticle weight percent and the purity of the nanofluid are analyzed as part of the nanofluid characterization. An Inductively Coupled Plasma Optical Emission Spectrometer (ICP-OES) is used for this purpose. The ICP consists of a plasma torch, load cell, tubes that carry the inert gas Argon, and a radio frequency generator. This machine is useful for this experiment because no addition sample preparation is required and each analysis takes only a few minutes, provided that proper calibration has been performed. The ICP is able to identify low elemental concentrations in fluid samples, down to ppb level (parts per billion) [13]. The ICP machine is able to find the elemental concentrations in a test sample by heating it up with a plasma torch. This forces the atoms to produce one or more specific wavelengths of light emission.

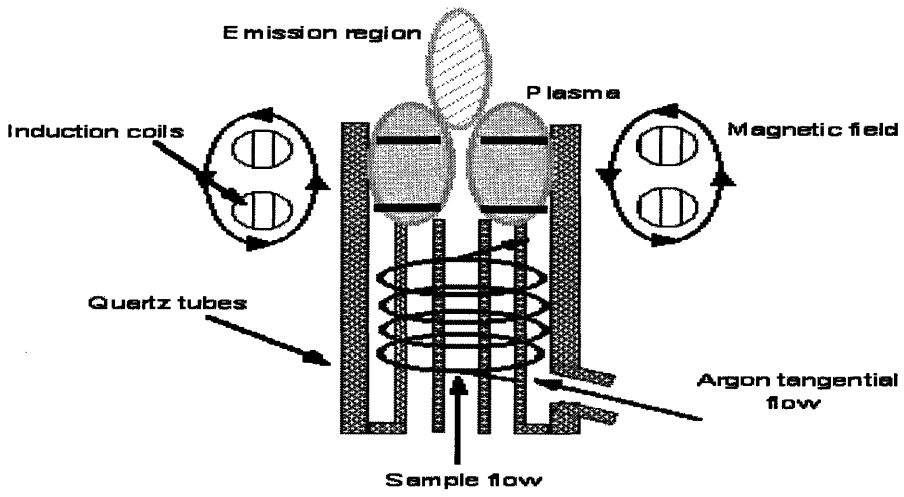


**Figure 2.1: Schematic of the inside of ICP machine (Courtesy of Science Hypermedia)**

Before test were done directly to the alumina test sample, there are standard solutions prepared at several ppm (parts per million) ranges in order to establish a calibration curve for the element of interest. The standards used were 0 ppm, 1 ppm, and 100 ppm of aluminum. This enabled data interpolation from intensity of a given wavelength to obtain the elemental concentration. The next step processed after this included making dilutions of the 8 samples taken before and after each weight percent run of the alumina nanofluids. The samples were diluted to fit the middle of the calibration curve, which is 50 ppm. In order to get dilutions of alumina on the 50 ppm scale, calculations of total alumina in samples are taken. The chemical formula used to help estimate the amount of aluminum in alumina is $Al_2O_3$. Using the atomic weights of aluminum 26.98154 and Oxygen 15.9994, it is found that there is approximately 53% of aluminum in alumina. The next step taken in the dilution process involves multiplying the percent of aluminum by the weight percent of alumina. Multiplying the results by one million will give a value of the amount of aluminum in ppm. The following formula is

used for finding the amount of concentrated nanofluid to add in order to obtain a diluted nanofluid:

$$\frac{DesiredPPM}{Metal_{PPM}} = \frac{X}{Water_{DesiredVol}} \tag{2.4}$$

Where DesiredPPM is the expected ICP ppm range that one wishes to use, $Metal_{PPM}$ is the amount of metal in solution in units of ppm, $Water_{DesiredVol}$ is the amount of water one uses to dilute the test sample. X is the amount of test sample solution.

## 2.3 QUALITATIVE STABILITY TESTING PROCEDURES

Below are series of simple lab tests performed to determine whether the nanofluids in question are able to remain stable at experimental testing conditions. These are dilution test, constant temperature test, and settling test.

### 2.3.1 Dilution Test

DT1. In this test, the nanofluid is diluted down with de-ionized water. This is done to imitate the dilutions that are made for the experimental test in the flow loop. This gives an idea whether there will be agglomeration upon dilution.

DT2. After the desired dilutions are made, then the small container that the samples are stored in is shaken up and placed in a small Petri Dish. A Petri dish is a clear glass or plastic dish. It is important that there is a small film layer at the bottom of a transparent Petri Dish, in order to make accurate measurements.

DT3. The Petri Dish is then raised to the light and observed from the bottom. This is where it can be noticed if there is any agglomerations because there will be particles that

are visible to the naked eye. If this is the case, then agglomeration was found after dilutions were made.

DT4. During the observation phase, it should be noted that whether any visible changes in the nanofluid can be seen. These observations may include a change in viscosity of the fluid or significant sedimentation of the particles.

### 2.3.2 Constant Temperature Test

CT1. This test is performed if the dilution test shows no visible settlement in the nanofluids. The diluted nanofluid is heated in a constant temperature hot water bath. This is to imitate high temperature conditions found in the experiment. This also aids in deciding whether there will be agglomeration.

CT2. Once the diluted nanofluids are prepared, each sample is heated at a constant temperature in the hot bath up to the maximum temperature (<90 °C) expected in the loop.

CT3. After the test sample has been sufficiently heated, then the same steps that were taken to observe agglomeration using the Petri Dish are completed once again. The sample is poured into the Petri Dish and is then observed from the bottom of the Petri Dish to find any visible agglomerates of nanoparticles.

### 2.3.3 Settling Test

ST1. This last test requires the nanofluid sample to be diluted and then subjected to elevated temperature. Higher temperatures were used because the nanofluids would be

subjected to similar conditions in the laminar flow loop. The purpose of this test is to determine how long it takes until the nanofluids in question settles.

ST2. These test samples remain in a stationary position and are observed periodically and then examined daily.

## 2.4 OBSERVATIONS

The NYACOL alumina nanofluid has been used in both pool and flow boiling experiments in our lab and have shown to be stable after dilution and when exposed to elevated temperature. Therefore it is determined from previous experience that alumina should remain stable under all conditions of the laminar flow experiments. The stability tests were performed for zirconia procured for this study, since NYACOL recently changed their production process for this nanofluid. Zirconia samples were diluted to four different concentrations from the as-received concentration of 12.8 weight %. These concentrations are 7, 3.5, 1.75, and 0.1 weight percent. No settling was observed in the conditions at ambient temperature. These samples were then heated to 90 °C in a constant temperature water bath. The samples were inspected about once per hour during a total period of about 6 hours. The transparency and the coloration of the nanofluids were unchanged. These zirconia samples were then allowed to settle for a 24-hour period. At the end of this period, the specimen showed signs of sedimentation. The nanofluid became more opaque near the bottom and there were agglomerates visible to the naked eye found in all the concentrations. When shaken in the test tube, the agglomerates disappeared. It was judged that, as long as the nanofluids are circulated and remained in

the loop for less than a day, sedimentation will not become a problem for the laminar flow experiments.

# CHAPTER 3

# DESCRIPTION OF EXPERIMENTAL FACILITY

## 3.1 LAMINAR VS. TURBULENT

There are three different flow regimes of concern when working with fluids. These are turbulent, laminar, and transitional region. Transitional flow exists between laminar and turbulent regimes. Determination of the flow regime can be related to the Reynolds Number:

$$\mathrm{Re} = \frac{\rho v D_{inner}}{\mu} \tag{3.1}$$

where $\rho$ is the density, $v$ is the mean flow velocity, $\mu$ is the dynamic viscosity of the liquid, and $D_{inner}$ is the inner tube diameter. Reynolds number is the ratio between inertia force and viscous force. When the Reynolds number is higher then 4800, the flow is turbulent [14]. Re between 2100 and 4800 corresponds to the transitional regime, i.e., the flow is in transition to the turbulent domain. Flow is best described in stream lines. The streamlines of turbulent flow are chaotic in nature as shown in experiments done by Osbourne Reynolds [14], where he injected a dye through a glass tube that enabled him to view the nature of flow at different pipe and flow characteristics. With Reynolds's experiment, it was discovered that turbulent flow has velocity fluctuations that causes the streamlines to move in an erratic matter. This allows the dye to be dispersed in the flow.

Laminar flow, however, is very different. The streamline for laminar flow is steady and smooth. In fully-developed laminar flow the velocity profile is parabolic. The

Reynolds number that is needed to maintain a laminar flow is normally under 2100. This occurs with the combination of high viscosity and low density, velocity, and inner tube diameter.

### 3.1.1 Laminar Flow Heat Transfer

Heat transfer in laminar flow regime can be solved analytically as described in [15]

There are two types of boundary conditions that lead to two different analytical solutions. The first one is a constant surface temperature. The analytical solution for constant surface temperature is derived from the differential energy equation:

$$\frac{\partial^2 t}{\partial^2 r}+\frac{1}{r}\frac{\partial t}{\partial r}=\frac{u}{\alpha}\frac{\partial t}{\partial x}-\frac{\partial^2 t}{\partial x^2} \tag{3.3}$$

In this energy equation t represents the temperature; r is radius, u velocity, x distance, and $\alpha$ the thermal diffusivity, which is defined as:

$$\alpha=\frac{k}{\rho * c_p} \tag{3.4}$$

Equation 3.3 can be re-arranged with dimensionless variables:

$$\frac{\partial^2 \theta}{\partial r^+}+\frac{1}{r^+}\frac{\partial \theta}{\partial r^+}=(1-r^{+2})\frac{\partial \theta}{\partial x^+} \tag{3.5}$$

Here θ is the non-dimensionless temperature and $x^+$ is the non-dimensionless distance. For a circular tube $x^+$ is defined as:

$$x^+=\frac{x/r_0}{\mathrm{Re}\,\mathrm{Pr}} \tag{3.6}$$

Equation 3.6 is solved using the boundary condition of constant surface temperature to give a formula in the following form:

$$Nu_x = \frac{\sum G_n \exp(-\lambda_n x^+)}{2\sum (G_n / \lambda^2{}_n)\exp(-\lambda^2{}_n x^+)} \tag{3.7}$$

At infinite distance, or fully developed laminar flow, Nu equals 4.36. The second condition that leads to an analytical solution for Nusselt number is constant heat flux. Using equation 3.6 the boundary condition for constant heat flux is used which gives the following formula:

$$Nu_x = \left[\frac{1}{Nu_\infty} - \frac{1}{2}\sum \frac{\exp\left(-\gamma^2{}_m x^+\right)}{A_m \gamma^4{}_m}\right]^{-1} \tag{3.8}$$

The formula above gives rise to a table that is used to find the Nusselt number throughout the entire length of the pipe. The results are displayed in the table below and the conditions are used in the following experiment.

Table 3.1: Nusselt number for a pipe with constant heat flux (Adopted from [15])

| $X^+$ | Nusselt Number |
|---|---|
| 0 | ∞ |
| 0.002 | 12 |
| 0.004 | 9.93 |
| 0.01 | 7.49 |
| 0.02 | 6.14 |
| 0.04 | 5.19 |
| 0.1 | 4.51 |
| ∞ | 4.36 |

### 3.1.2 Laminar Flow Friction Pressure Loss

There is a friction factor $f_f$ that is used to determine the pressure drop at different flow regimes. The equation for the friction factor in fully-developed laminar flow is $f_f = \frac{64}{\mathrm{Re}}$. This can be found using the Moody chart, which uses Reynolds number to find different friction factor for various surface roughness.

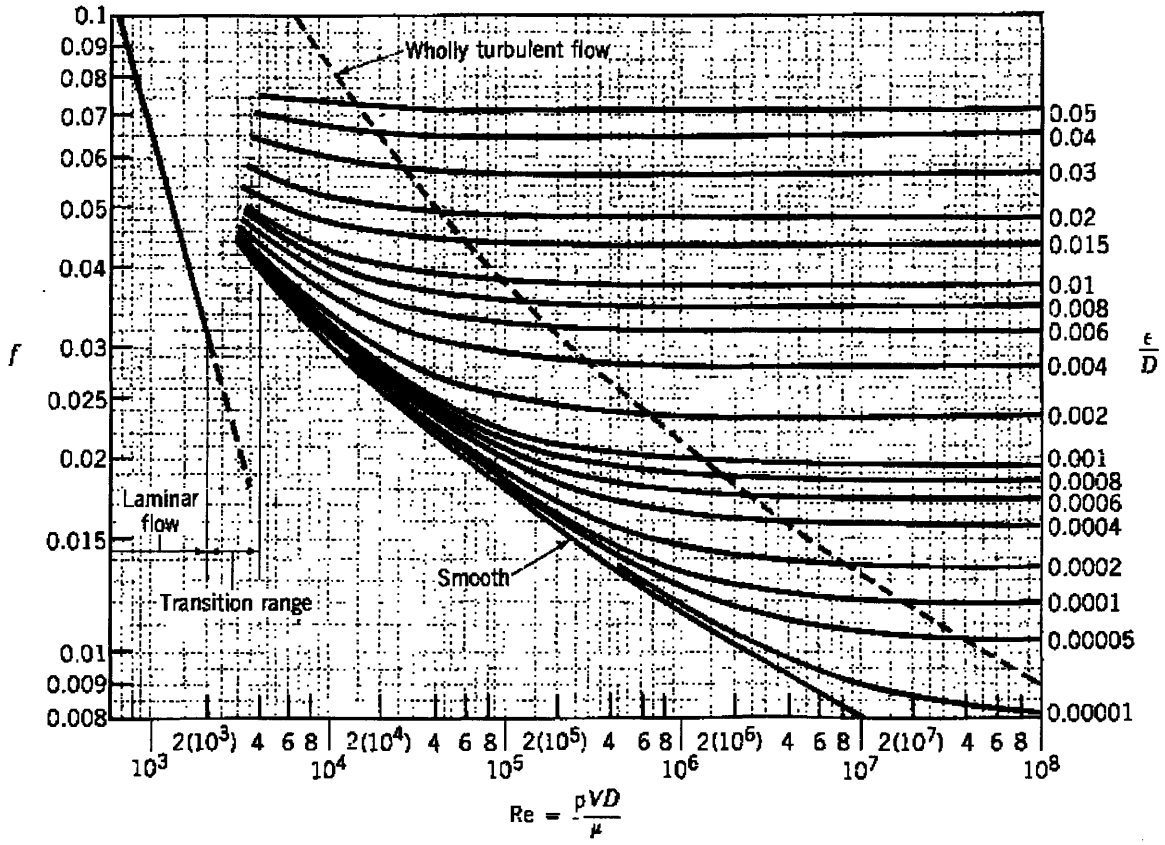


**Figure 3.1: This is a picture of a moody chart, used to identify friction factor at different Reynolds number (Adopted from [14])**

The objective of this study is to measure the heat transfer coefficients and pressure drop of nanofluids in the laminar flow regime. It is important to ensure that the design of the experiment will allow a wide operating range within the laminar flow

regime. Furthermore it is also imperative to verify the design criteria are met for both pure water and nanofluids because the thermophysical properties of concentrated nanofluids may vary significantly.

## 3.2 APPARATUS

There are several key components attached to the single-phase laminar loop. These include data acquisition system, thermocouples, gear pump, heat exchanger, cool water bath/chiller, flow meter, power supply, and pressure transducer.

### 3.2.1 Data Acquisition System

The data acquisition system uses waves and signals to convert data from the loop to the computer. The type of data acquisition system used is the HP3852A. This type of data acquisition system can handle a variety of transducer inputs. These include thermocouples, transducers, and measurements in DC voltage, current, resistance, frequencies, and pressures. This is sufficient to measure data for the experiment in the loop.

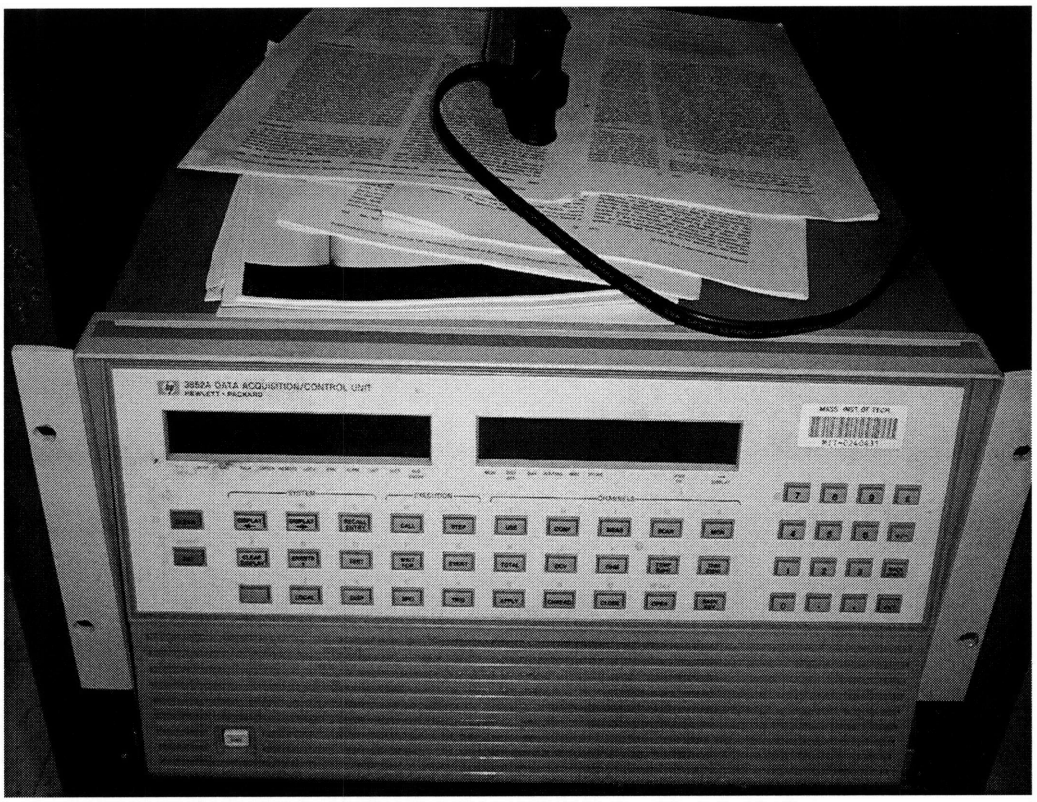


**Figure 2.2: Picture of the data acquisition system used to process data from experimental instruments**

### 3.2.2 Flow meter

The flow meter is used to measure the volumetric flow rate of the fluid. The flow meter used in the laminar loop experiment is the FTB9504. The FTB9504 is used to measure the extremely low flow rates expected in laminar flow, i.e., from 0.013 to 0.264 gpm in our case. The flow meter uses a rotor that is similar to a wheel. The rotor is moved by the fluid and the rotation frequency is converted to flow rate via calibration. A 20 point calibration curve was provided by the flow meter vendor. A 20 point curve is a set of parameters that the company uses to test where the frequencies lie with respect to the flow rates. These calibrations are done to ensure that proper flow rates are read.

### 3.2.3 Thermocouples

Thermocouples are used to measure temperature. K-type thermocouples were used for this experiment. The K-type thermocouple uses Chromel alloy [1] and Alumel alloy[2]. The thermocouples run in the -200 to 1250 °C ranges. The K-type thermocouple has an accuracy of +/- 1.1 °C and a resolution of 0.37 °C. [16]

### 3.2.4 Heat Exchanger

The heat exchanger removes heat from the system to make sure that overheating does not occur. The heat exchanger in the laminar loop is made with copper tubing coiled tightly inside a plastic bottle which holds secondary coolant.

### 3.2.5 DC Motor Gear Pump

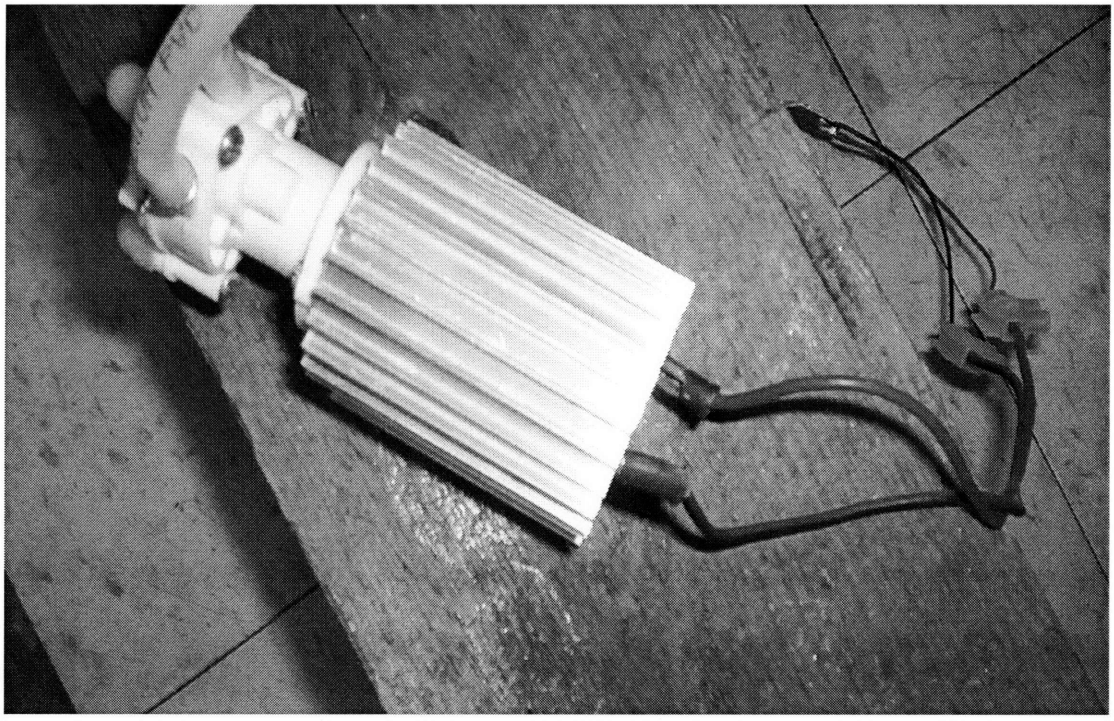

**Figure 3.3: Picture of gear pump used to circulate the fluid throughout the loop**

[1] Chromel alloy is made of nickel and chromium
[2] Alumel alloy is made of aluminum and nickel

The gear pump is another essential apparatus to the smooth running of the flow loop. This type of pump has two internal gears. When the gears start moving in the presence of fluid, they push the liquid through the small gear teeth. It is important that the pump is run with a DC motor, as alternating current may cause fluctuations of power, which in turn would affect the flow rates of the fluid. The gear pump used in the experiment uses a small DC motor that works constantly at 12 Volts.

### 3.2.6 Cool Water Bath (Chiller)

The cool water bath/chiller is another method to remove heat from the fluid. It works with the heat exchanger. The cool water bath/chiller has water with a metal coil inside that function to keep the water cold. The test fluid arrives in the cool water bath and exits the cool water bath with a lower temperature. This is used to control $\Delta T$, defined as the difference between $T_{outlet}$[3] and $T_{inlet}$[4].

### 3.2.7 Differential Pressure Transducer

The pressure transducer is an important device in the loop. It is able to measure the pressure drop difference between two points in the loop. The transducer used for the loop is the PX154-001DI from Omega Engineering. The conversion of pressure into an electrical signal is achieved by the physical deformation of strain gages which are bonded into the diaphragm of the pressure transducer and wired into a Wheatstone bridge configuration. Pressure applied to the pressure transducer produces a deflection of the diaphragm which introduces strain to the gages. The strain will produce an electrical

---

[3] $T_{outlet}$ is the temperature of the fluid as it exits test section.

[4] $T_{inlet}$ is the temperature of the fluid as it enters the test section.

resistance change proportional to the pressure. [19] The transducer was already calibrated to operate within 1% accuracy.


**Figure 3.4: Displayed above is the pressure transducer used to measure the pressure drop of the experimental loop**

### 3.2.8 Function and Schematic of Loop

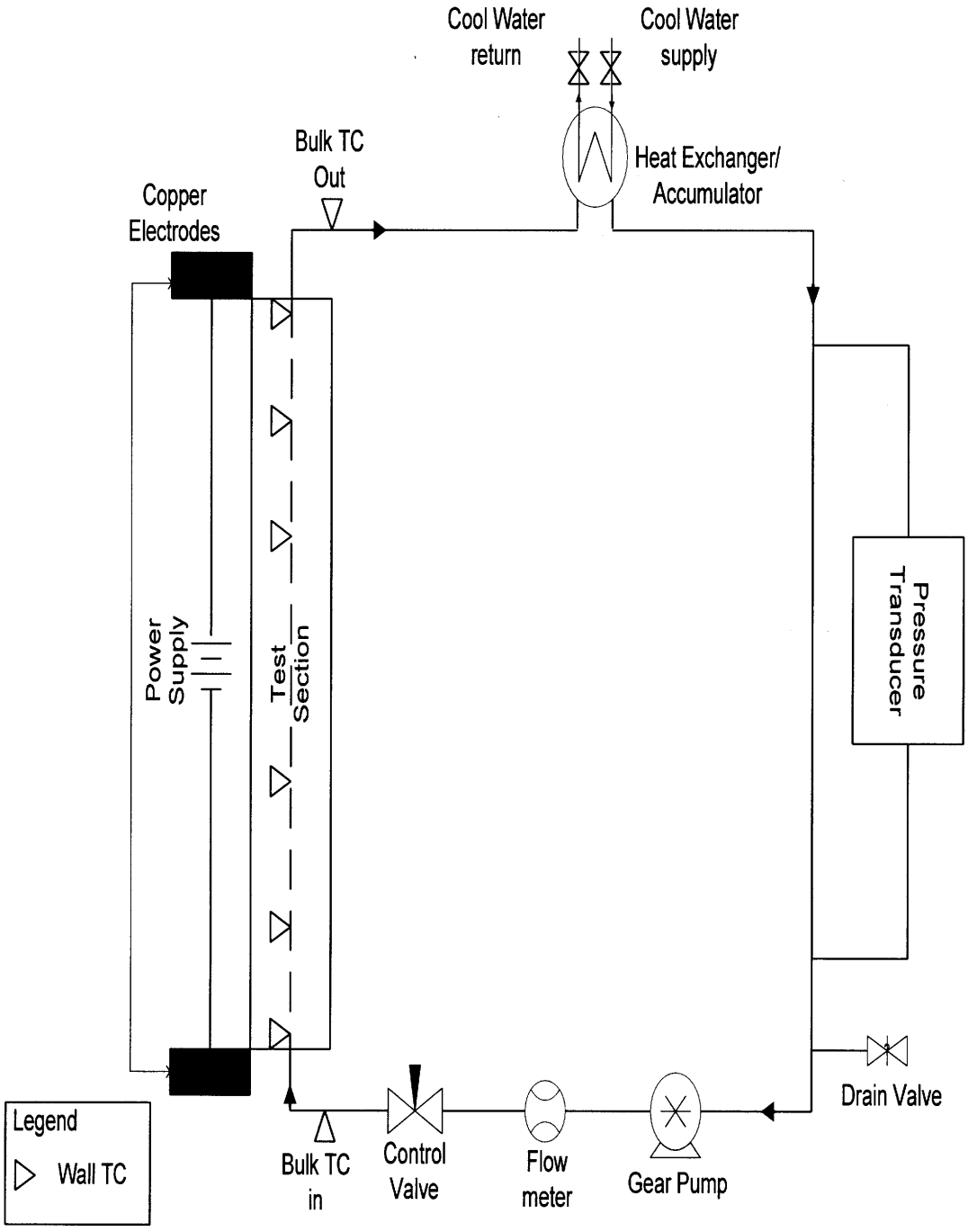


**Figure 3.5: Schematic of experimental loop**

A schematic of the experimental apparatus is shown in Figure 1. The experimental loop was designed for convective heat transfer in the laminar flow domain. It was constructed with stainless steel tubing. The flow meter was positioned just after the pump discharge. The vertical test section was a stainless steel tube with an inner diameter (ID) of 4.5 mm, outer diameter (OD) of 6.4 mm, and length of 1.01 meters. The test section had eight sheathed and electrically insulated K-type thermocouples soldered along the test section and two similar K-type thermocouples inserted into the flow channel before and after the test section to measure the bulk fluid temperatures. These thermocouples and the flow meter provided the data to determine the thermal power of the experimental loop.

$$Power_{Therm} = C_p * (T_{out} - T_{in}) * Q * \rho \tag{3.9}$$

Where $C_p$ is the specific heat of the nanofluid, $T_{out}$ is the bulk outlet temperature, $T_{in}$ is the bulk inlet temperature, Q is the volumetric flow rate, and $\rho$ is the density of the nanofluid The test section used in the experiment was resistively heated by a Sorensen DCR 20-125 DC power supply. This power supply has a DC output rating of 0 to 20 volts and current of 125 amps. After being heated the fluid was cooled using a chiller that provided flow to a coil placed in the accumulator. The chiller was a Polyscience recirculation chiller, model #1175P. After the test fluid was cooled, it ran through a 1.45 m long and 5.8 mm ID vertical isothermal section where the pressure drop was measured by an Omega PX 154-001DI pressure transducer, able to read up to 1 inch (2.54 cm) of water with an accuracy of 1% of the full scale. A HP3852A data acquisition system controlled by a visual basic program was used to record the output of all instrumentation.

Additional loop components included a needle valve to control the flow rate throughout the loop and a drain valve.

## 3.3 SELECTION OF HEATED LENGTH

Deciding the heated section length is important for the success of the experiment. The heated length ensures that the flow in the experiment is fully developed. There are many considerations to take into account before making this decision. Figure 3.6 shows the velocity distribution of laminar flow in developing and fully-developed regimes.

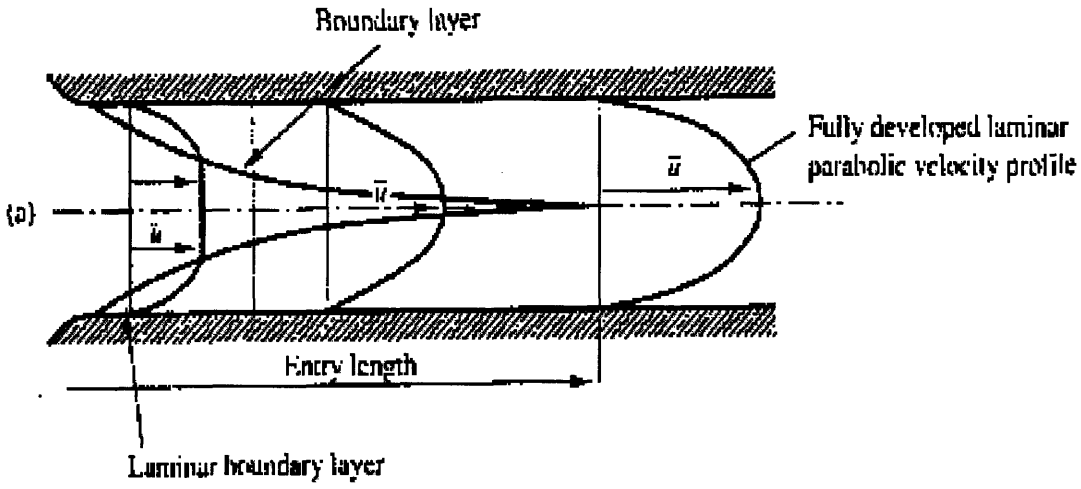


**Figure 3.6: This schematic displays the different velocity profile from the entrance region to a fully developed flow. Courtesy of Cartage [18]**

It can be seen from the diagram that the entrance region velocity profile is relatively flat. The boundary layer at this point is negligible. Further downstream, the boundary layer forms on the inside surface area and start to take up a larger part of the area as the flow continues throughout the pipe. When the boundary layer thickness reaches the pipe radius, then the flow is considered to be fully-developed.

The entrance length for velocity profile is dependent on Reynolds number:

$$\frac{L}{D} \approx 0.06 * \mathrm{Re} \tag{3.10}$$

where L represents the entrance length, or the length in which the flow becomes fully developed, D represents the inner tube diameter, and Re is the Reynolds number. To estimate the appropriate heated section length, a Re of 2100 was used. This led to an entrance length of 126 diameters until the flow became fully developed. The heat convective loop used an inner diameter of 4.45 mm. For the purpose of this experiment, a heated section length of 1.011 m was chosen. Note that the thermal entrance length is different from the velocity entrance length. The thermal entrance length is a function of Prandtl number and Reynolds number as shown in equation 3.6. The velocity entrance length is used here for an approximation for the heated test section length selection.

## 3.4 PRESSURE TRANSDUCER TUBE SELECTION

The pressure drop is estimated in order to select a pressure transducer of the appropriate operating conditions. The pressure drop is calculated by using the following formula:

$$\Delta P = f_f * \frac{L}{D} * \frac{\rho v^2}{2} \tag{3.11}$$

Where $\Delta P$ the friction pressure drop, L is length of the tube, D is the inner diameter of tube, $\rho$ is the density of the liquid, $v$ is the velocity of the liquid and $f_f$ is the friction factor. For laminar fully-developed flow, the friction factor is:

$$f_f = \frac{64}{\mathrm{Re}} \tag{3.12}$$

In selecting the correct geometry for the tubing for the pressure transducer, the maximum pressure drop that the instrument can measure is taken into consideration. Following that analysis is considered through examining the extreme cases for each part of the experiment. This would mean the highest possible viscosity and flow rate that can be obtained without going over the Reynolds number is 2100. The unknowns for these conditions are the length and the inner diameter for the tube on the isothermal side. In order to find an appropriate parameter, one parameter needed to be assumed. The assumed parameter for this experiment was the diameter, since there is a limited choice of manufactured diameters. The following is a table of geometries decided upon:

Table 3.2: Tube Parameters (determined when Pressure Loss is 0.036 psi)

| Inner Diameter (inches - millimeters) | Length (meters) |
|---|---|
| 0.19 – 4.826 | 1.232 |
| 0.21 – 5.334 | 1.839 |
| 0.206 – 5.232 | 1.703 |
| 0.214 – 5.436 | 1.983 |
| 0.219 - 5.116 | 2.175 |

For the purposes of this experiment, a range of length and diameter values shown in table 3.2 were to be chosen. The choice was an inner diameter of 0.19 inches (4.826mm) and a length of 1.45 meters. These dimensions were chosen allow some margin of error between the operating pressure and the upper limit of the pressure transducer.

# CHAPTER 4

# LAMINAR LOOP OPERATING PROCEDURES

## 4.1 PREPARATION

P1. Prior to experimentation, the experimental setup is checked. The nozzle is checked to make sure that it is all the way open. (Note: If the nozzle is completely closed then once the pump is turned on then the tube would blast off the pump because of the sudden increase of pressure once the pump is turned on when the nozzle is near shut.)

P2. The accumulator is then checked to make sure that the loop is filled with DI water or nanofluid. The accumulator must have fluid in it because if the accumulator is empty, then the pump can be damaged because it was made to handle liquids and not air flowing through the pump. The amount that is placed in the accumulator for this experiment is about three liters. When dilutions are made with the nanofluids in the loop, the weight percent is reduced by half its initial weight percent. This is accomplished by draining half the volume of nanofluid and replacing the volume drained with de-ionized water.

P3. The power supply is then checked to make sure that the knobs are fully turned counter clockwise to make sure that there is no voltage or current running through the loop once the power supply is on.

## 4.2 LOOP OPERATION

O1 The data acquisition system would be turned on next. The data acquisition system is turned on by first connecting the GPIB port from the connector and then pushing the power button. This records all the signals into the computer and is turned into

measurements. Visual Basic Program is turned on following the commencement of the data acquisitioner. Once the Visual Basic Program is on, it gives a reading of the various measurements of concern in the loop to make sure everything is in order. It is then able to record and observe the experiment in the beginning phases.

O2. The pressure transducer is to be checked to see if there is any air in the system because the pressure transducer measures one inch of pure water flow. If there are any air bubbles in the tubing, then the pressure measurements that are sent through the data acquisitioner to the computer become questionable. The steps taken to take out the air involve using a wrench and loosening the nuts on the tube closest to the pressure transducer so the water leaks out. Once the air is no longer seen through the loop then the nut is retightened. $\Delta P$ is then measured and recorded at zero flow rate. This is important because the pressure transducer is sensitive and operates at a low pressure ranges. The pressure may be off due to not being placed on an even surface.

O3. The pump is turned on by sliding the lead onto the pumps electrical clips. Then the pump is allowed to run for approximately an hour. The pump is run for this long because it needs to be assured that the flow remain constant. This is done by checking that the standard deviation of the flow rate is lower than 1% of the total flow rate.

O4. Cool water bath is connected to the tubes that extend from the heat exchanger. This is connected and used to make sure that the flow of water that enters the test section is cooled. The cool water bath's settings are placed so that the temperature reads around 2 degrees Celsius. It is important that the temperature settings do not fall below 2 degrees Celsius because it may freeze over. This would lead to problems for the loop.

O5. The gear pump is turned on, and from there the desired flow rate is then obtained by throttling the valve.

O6. The power supply can now be made operational. The power that is chosen is depended on the setting of the flow rate. The settings are chosen so that the inlet temperature and outlet temperature at the test section is approximately 10 degrees Celsius or higher.

O6. After the desired flow rate and/or heat flux is chosen, then steps are taken to begin the experimentation. Then the loop must be left idle until the temperature reach a quasi-steady state. For the purpose of this experiment, thermal equilibrium takes approximately ten minutes. Once the temperature has ceased its fluctuation then it can be seen that the flow has reached steady state.

O7. After the flow has reached steady state, then a filename can be taken using the Visual Basic Program. Once the file name is given, then results can be taken. The loop runs for approximately 2 minutes and data points are taken roughly every 2 seconds in pressure, voltage, current, flow rate, heat flux, and temperatures at various positions on the test section.

O8. Once a complete run has occurred for nanofluids at different weight percents, a 50-milliliter sample is taken after the run for characterization purposes.

## 4.3 SECURING THE LOOP

After many trials are taken at different flow rates and heat fluxes are obtained, then shutting down procedures can take place.

S1. Proper shutdown begins with shutting down the power supply. This is first because this is the main component that is supplying heat to the entire loop.

S2. The nozzle is set fully open to allow maximum flow rate and cool water to circulate through the system faster.

S3. Then the loop is left idle for approximately 10 minutes with the cool water bath still on because the water needs to be cooled close to room temperature especially if high temperatures were used in the experiment.

S4. Turn off pump

S5. The cool water bath is then turned off and detached from the loop. After one last check is made to make sure that the temperatures and the loop's apparatuses are in order, then data analysis of the results can take place.

S6. The loop is removed of nanofluids via the drain valve. The purpose of this is to ensure that there are no nanofluids settling in the experimental loop. This settling would cause inadequate data upon ensuing usages and possible clogging and corrosion of the apparatus.

## CHAPTER 5

## TEST MATRIX

In this study, de-ionized water, alumina nanofluid and zirconia nanofluid are tested in the loop. The purpose for testing de-ionized water is to provide accurate knowledge that the test is consistent with analytical solution as shown in chapter 6, and then a proper comparison can be made to that of the nanofluids. Tests are to be done to obtain the Nusselt number versus the dimensionless axial coordinate $x^+$. The thermophysical properties needed for data analysis are specific heat, density, thermal conductivity and viscosity. These properties are temperature-dependent and vary with the type and concentration of nanofluids. Thermal conductivity and viscosity of alumina were characterized and modeled by Williams [3]. Although these were also measured previously for zirconia by Williams, Nyacol had since utilized a different preparation method for the current batch of zirconia nanofluid and therefore it was determined that thermal conductivity and viscosity of zirconia need to be re-analyzed.

The following formula is for nanofluid specific heat.

$$c_{mix} = \frac{((1-Vol\%)*\rho_f*c_f)+(Vol\%*\rho_s*c_s)}{\rho_{mix}} \tag{5.1}$$

The variable c represents specific heat, $\rho$ density, and the subscripts $f$ represents fluid and s the actual nanoparticles. The density equation used can be found in Chapter 2 Equation 2. The viscosity and thermal conductivity property equations of Alumina were found using the correlations formulated by Williams. Since this test uses the same vendor, Nyacol, as Williams for experimentation, the property equation do not

need to be recreated. Utilizing Williams' viscosity for Alumina, the following formula is used [6]:

$$\mu_{mix}(T) = \mu_f(T) * \exp\left(4.91 * \frac{Vol\%}{0.2092 - Vol\%}\right) \tag{5.2}$$

The mixed viscosity, $\mu_{mix}$ changes depending on the temperature conditions of the base fluid's viscosity, $\mu_f$ which the test is running at. The thermal conductivity equation used for alumina is as follows:

$$k_{mix}(T) = k_f(T) * (4.5503 * Vol\% + 1) \tag{5.3}$$

The mix thermal conductivity, $k_{mix}$, is dependant on the base fluid's thermal conductivity, $k_f$. Tests were completed writing down systematically before hand the range of flow rates that maintained laminar Reynolds number for de-ionized water and each concentration of nanofluids. This was to ensure unexpected problems later if a test is found to be in the turbulent domain.

The Nyacol vendor was used in experimentation with zirconia. The method used to make the zirconia was different then that used in Williams' experiment. The thermal conductivity is estimated to be approximately the same due to the same metallic particles being distributed throughout the base fluid. The correlation used for zirconia's thermal conductivity was used based on the measured results being similar to Williams' correlation, which is:

$$k_{mix}(T) = k_f(T) * ((-29.867 * Vol\%^2) + (2.4505 * Vol\%) + 1) \tag{5.4}$$

When Williams' viscosity correlation was used to determine the Reynolds number and find the pressure loss, discrepancy was found in the data. The viscosity for zirconia needs a new property equation to use due to the new method to stabilize the zirconia

particles in the fluid. Experimental data was then taken at three different concentrations at two different temperatures. The concentrations used were 12.8, 7, and 1.7 weight percent. The results were graphed with viscosity measured divided by viscosity of water versus the volume fraction.

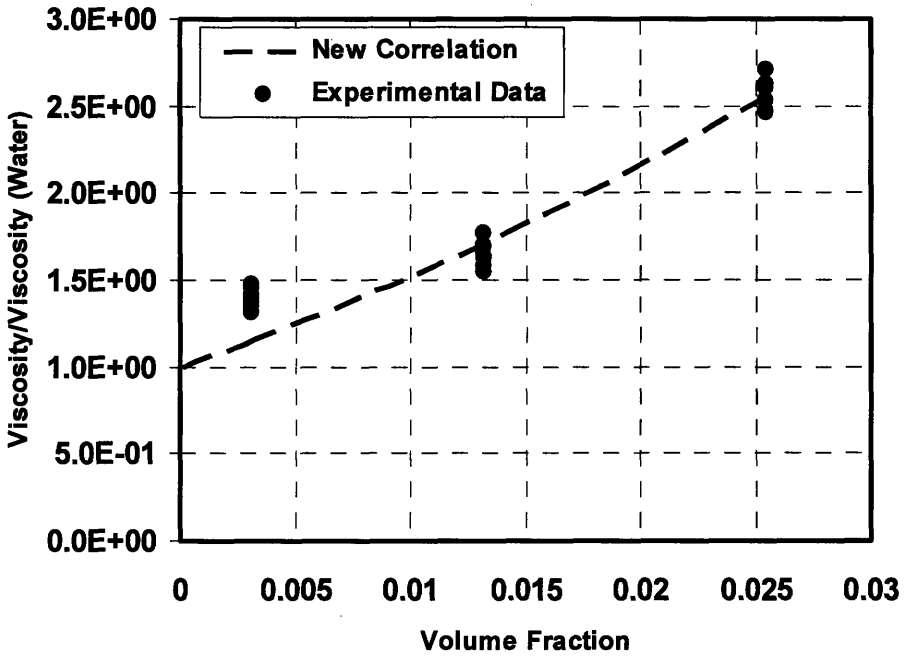


**Figure 5.1: Shows the trend line that fits the data that was found using the viscometer.**

This data gives the following correlation for the viscosity of zirconia:

$$\mu_{mix}(T) = \mu_f(T) * \left[(550.82 * \phi^2) + (46.801 * \phi) + 1\right] \tag{5.5}$$

This new correlation was compared to the one that Williams used in his experiment at varying volume percent. This is displayed on the tables below:

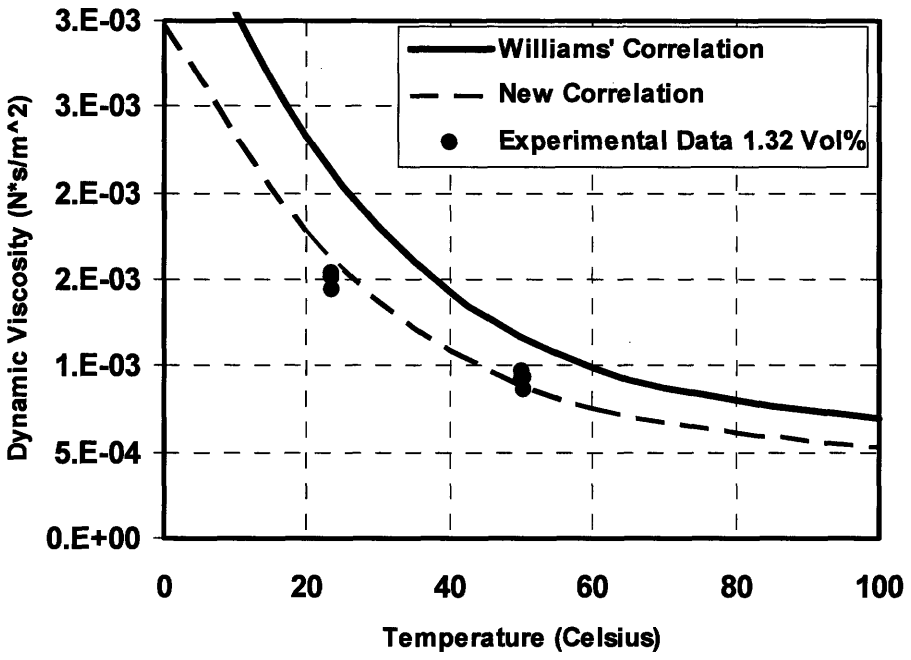


Figure 5.2: Displays the Williams and the new correlation at 1.32 volume %

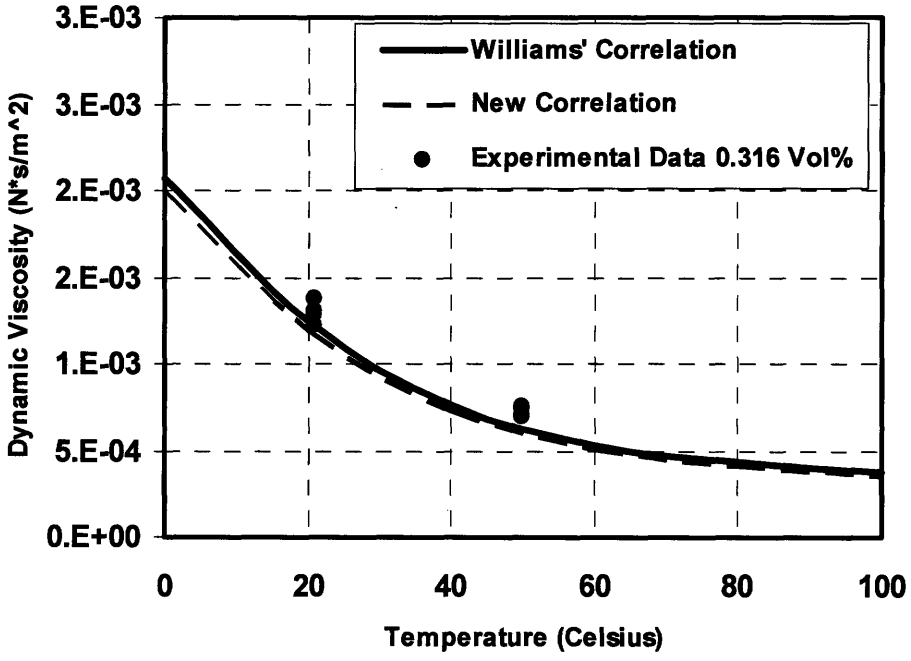


Figure 5.3: Displays the Williams and the new correlation at 0.316 volume %

When this new property equation was implemented into the results that were taken, the pressure loss and Reynolds number values became more reasonable. This was to ensure correct estimations of which flow domain the experiment is run at.

After the new property equation was made, the following information was recorded:

Table 5.1: Test Matrix

| DI Water | Test # | Date | GPM | Heat Flux | Weight % | T diff | Comments |
|---|---|---|---|---|---|---|---|
| Alumina | Test # | Date | GPM | Heat Flux | Weight % | T Diff | Comments |

The test matrix has a comment column where usually pressure difference at no flow rate is measured in order to give accurate pressure difference data. The temperature differential column is added to ensure that there is around 10 degrees Celsius difference or error in results may occur.

# CHAPTER 6

## 6.1 DI WATER VALIDATION TESTS

DI water was tested prior to nanofluid runs in order to make sure the experimental facility and instrumentations operate as expected. Testing for water is done from several different flow rates, which gives a range of Reynolds number that are below 2000. These runs found estimated pressure and Nusselt number values for DI water in laminar flow.

The first ten de-ionize water experiments found a Nusselt number at a range of flow rates that range from 0.02 gallons per minute to 0.08 gallons per minute. The Nusselt number for the fully developed laminar case is equal to 4.36.

These results display that the measured Nusselt number is lower than the theoretical values from Ref [14] by approximately half the Nusselt number. The discrepancy in theoretical Nusselt number and measured value gave reason to check several of the instruments that were on the experimental loop. This led to the purchase of a pressure transducer that would be able to test to see if the flow meter is in fact actually the main cause for error.

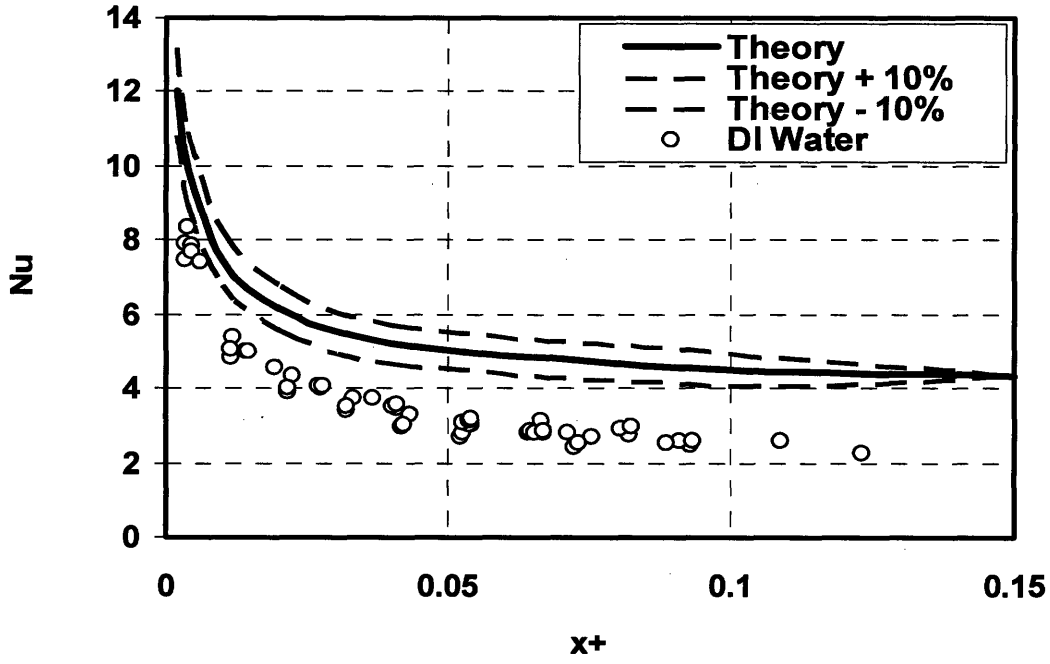


**Figure 6.1: The above graph displays all Nusselt Theory and Nusselt Measured number values from 11 DI Water runs with respect to the last local mean.**

In the first test of DI Water runs, there has been constant heat loss of around 30%. This constant value of heat loss gave a need to find a pressure difference for the experimental loop. The calibration of pressure difference was taken about a large range of flow rates from 0 to 0.25 GPM with increments of 0.05. The pressure is calculated using the formula from Eq. (3.10):

$$\Delta P = \frac{\rho * v^2}{2} * \frac{L}{D_{inner}} * \frac{64}{\mathrm{Re}}$$

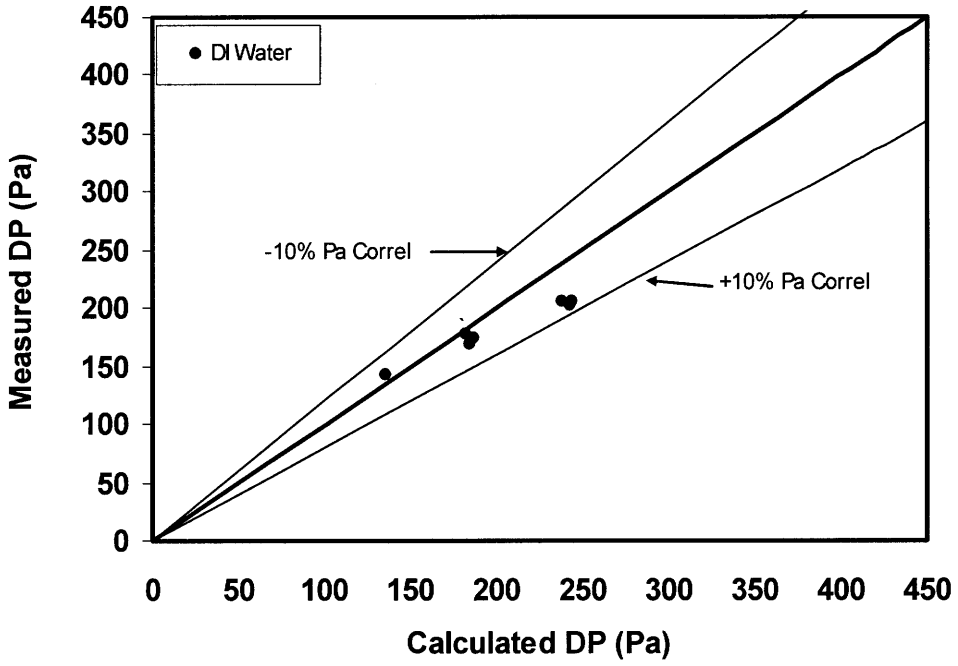


**Figure 6.2: The above graph shows the consistency of the measured pressure to calculated pressure with respect to flow rate**

The consistency displayed in the above graph suggests that there is no problem with the flow meter. The discrepancy in heat loss led to a closer look at the electrical power and the thermal power. The electrical power equation is:

$$Power_{Elec} = I * V \tag{6.1}$$

Where I is the current and V is the voltage, and the thermal power equation is:

$$Power_{Therm} = \dot{m} c(T_{Out} - T_{In}) \tag{6.2}$$

Where $\dot{m}$ the mass flow rate, c is the specific heat, $T_{Out}$ is the bulk outlet temperature and $T_{In}$ is the bulk inlet temperature. Since the electrical power and the thermal power were not similar then there had to be a problem with the thermocouple. The reason the

thermocouple was suspected was because the power supply was consistent with little error. It was found that the bulk outlet temperature was off by approximately 1 to 2 degrees Celsius. A new thermocouple replaced the bulk outlet temperature and was placed in a new position.

With the new thermocouple installed in a new location on the loop, more experiments were run using DI water. To verify that the new configuration works well, an additional testing of the pressure transducer was done between the flow rate of 0.02 and 0.05 GPM. The pressure of the DI Water is measured to ensure that there are no problems with the flow meter.

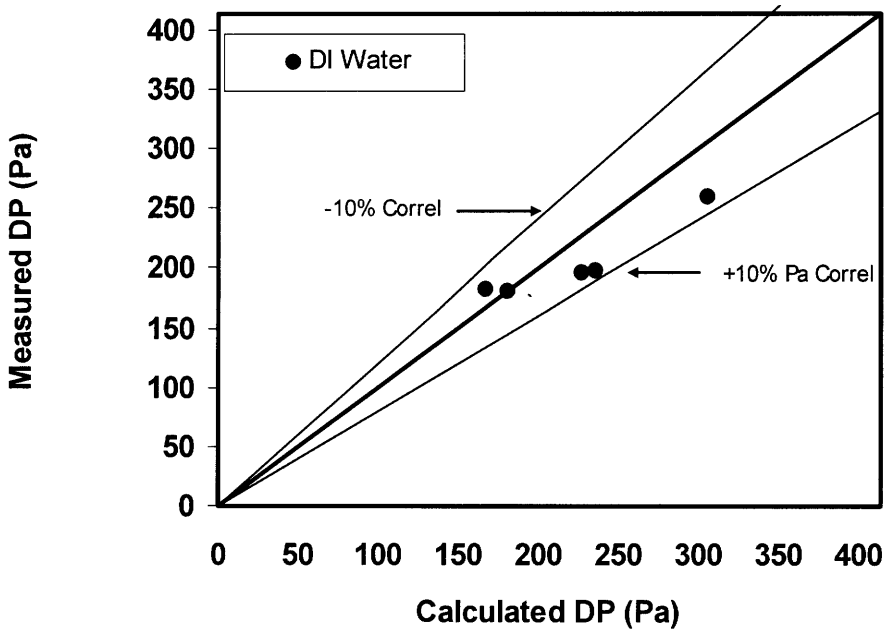


**Figure 6.3: The pressure calculated and measured after the new thermocouple was placed**

The pressure below is found to be within the range of plus and minus the 20% of measure and actual pressure, which display no major problems with the flow meter.

There were 12 experiments of DI water runs where the DI water was tested against the analytical laminar solution

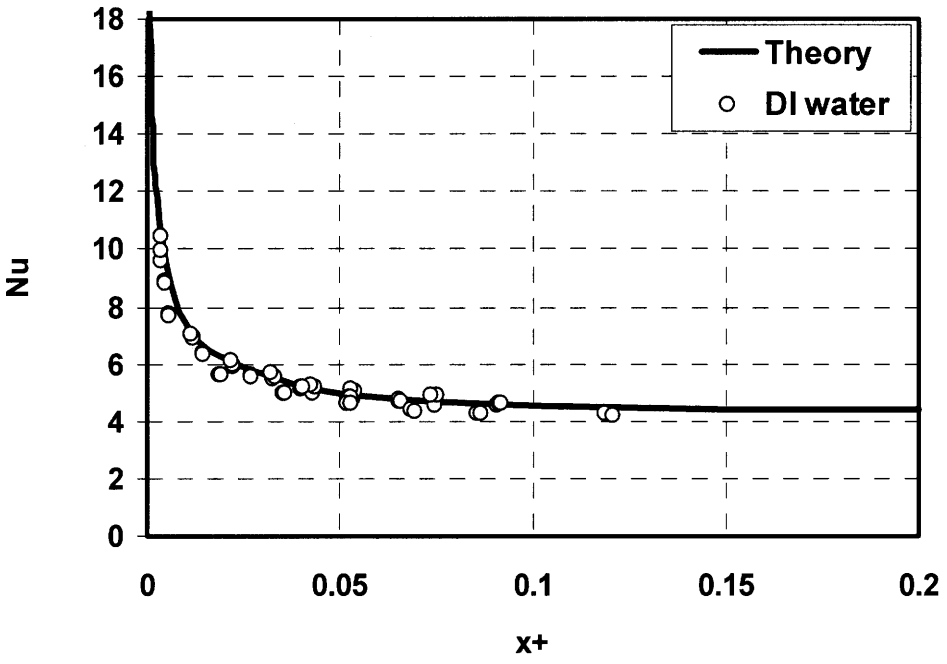


**Figure 6.4: The above graph gives the calculated and measured values of Nusselt number with respect to the local mean**

The above results are consistent with the measured Nusselt number and these results originate from DI water experiments 1 through 12. The measured Nusselt number is approximately same as the theory. This graph satisfies the result better with the new thermocouple. The heat loss was found to be approximately 10%, which is better compared to the 30% heat loss prior to the thermocouple location change.

## 6.2 ALUMINA TEST

Experimental observations were noted during the nanofluid runs. When experimentation occurred, the loop ran for approximately 1 hour preceding the first run. Once the runs began, it took 10 minutes between runs in order for steady state to occur. At the completion of the experimental runs, not all the data can be used. The reasons for this include Reynolds numbers that exceed 2100 and places the result in the turbulent domain. Data that is gathered with a heat loss that is higher than 10% are not used because of the low Nusselt number found. This was caused by the error increase that occurs when the flow meter reaches lower flow rates and its unstable flow rate results. In order to ensure that there were no problems with the loading and dilution procedures, ICP results were taken to corroborate the estimated weight percent results used in data analysis. A table of the alumina ICP runs is provided below:

Table 6.1: ICP Results for Alumina

| Alumina Test Sample | Test Sample Volume (μL) | Water Volume Used (mL) | Expected ICP PPM | Measured ICP PPM |
|---|---|---|---|---|
| 20 wt% Before | 47 | 100 | 50 | 48.676 |
| 20 wt% After | 47 | 100 | 50 | 48.82 |
| 10 wt% Before | 94 | 100 | 50 | 53.8 |
| 10 wt% After | 94 | 100 | 50 | 54.223 |
| 5 wt% Before | 188 | 100 | 50 | 44.2 |
| 5 wt% After | 188 | 100 | 50 | 44.66 |
| 2.5 wt% Before | 376 | 100 | 50 | 43.49 |
| 2.5 wt% After | 376 | 100 | 50 | 42.89 |

These results display that the weight percent estimated are trustworthy to use in future calculations because of the consistency of the results of the two runs used for each weight percent.

The alumina tests were done with 54 test ranging from 19.5, 10.8, 4.44, and 2.16 weight percent. The alumina's pressure and Nusselt number were taken with respect to the DI water, which is used to evaluate if there is any heat enhancement.

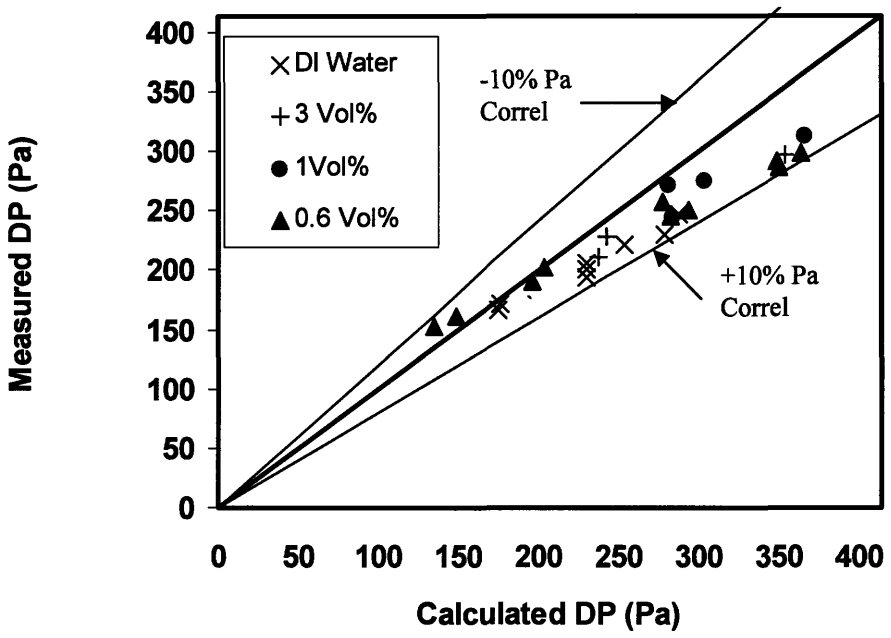


**Figure 6.5: This graph displays the list of the alumina and DI water runs expressing pressure loss**

The pressures are within the 20% boundary lines on the graph. This shows that there is no disagreement of results caused by the flow meter. It also displays the consistency of the nanofluid runs. The evaluation of the various weight percent of the nanofluid was the main focus of this study. The following graphs display the trend that alumina nanofluid holds with different concentrations.

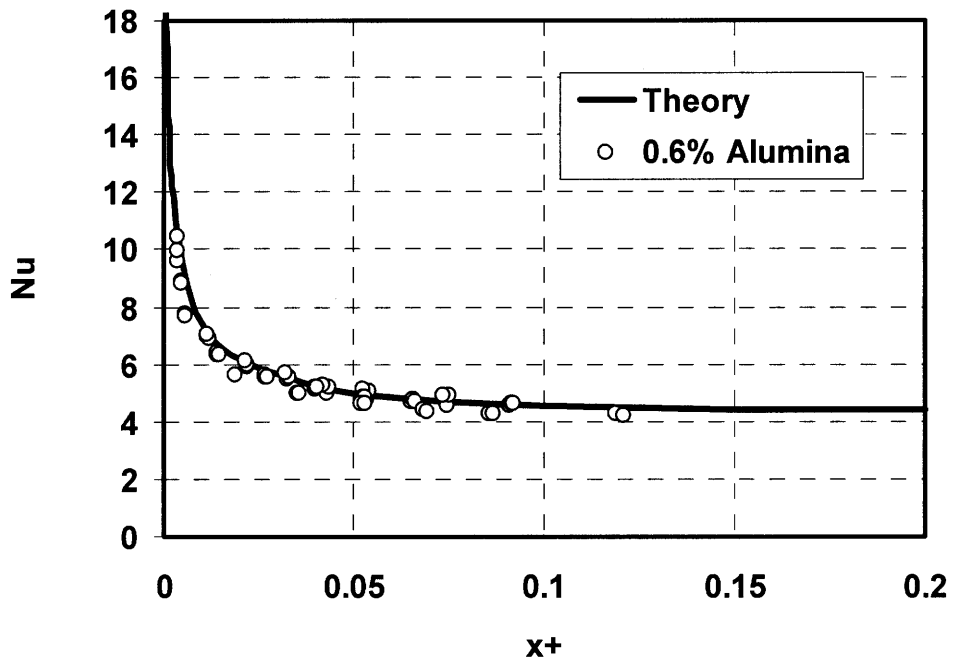


**Figure 6.6: This graph shows the consistency of the theory with Alumina at 2.16 Weight %**

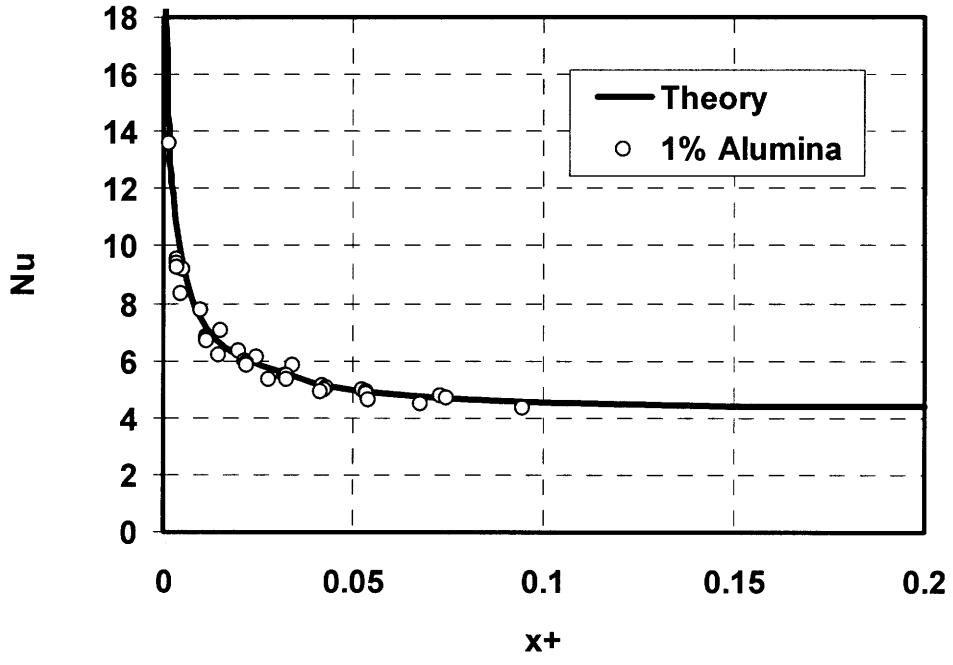


**Figure 6.7: This graph shows the consistency of the theory with Alumina at 4.44 Weight %**

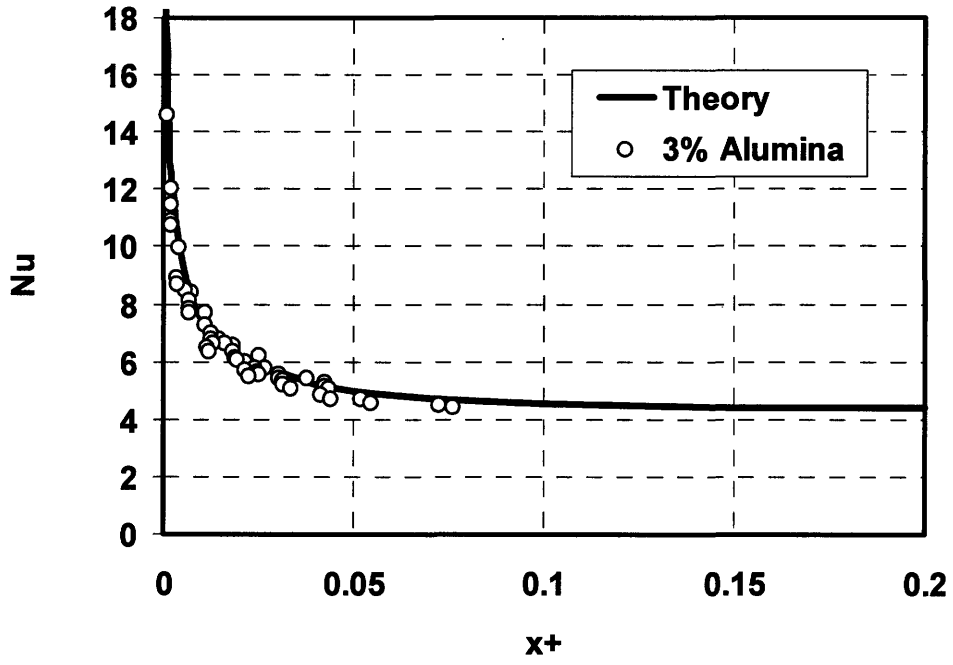


**Figure 6.8: This graph shows the consistency of the theory with Alumina at 10.80 Weight %**

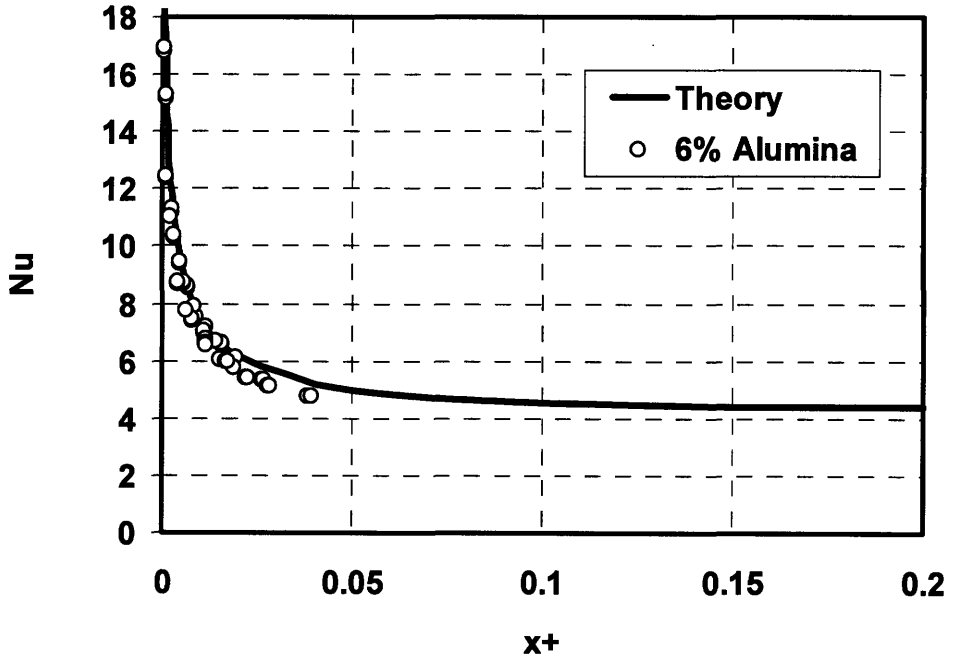


**Figure 6.9: This graph shows the consistency of the theory with Alumina at 19.50 Weight %**

The trend that involves the higher Nusselt number values found in the entrance region of the test section fits the theoretical prediction. The nanofluid fits perfectly with the theory, regardless of the nanofluid concentrations.

There is heat enhancement that is found in the entrance region of the test section based on the thermophysical properties of the nanofluid. In order to find this data, the heat transfer ratio is created with the heat transfer coefficient measured is divided by the calculated heat transfer coefficient. This is set-up versus the volume fraction of the nanofluid in question. The axial location is found to determine the heat transfer ratio from the following equation:

$$x^{+} = \frac{2 * \left(x/D\right)}{\mathrm{Re}^{*}\ \mathrm{Pr}} \tag{6.3}$$

[17] The Nusselt number used to find heat transfer is found with respect to the axial location found in the above equation. The axial location gives the distance of approximately the location of the entrance region. This is defined for when $x^{+} \leq 0.01$. The following formula is used to determine the Nusselt number calculated: [17]

$$Nu = 1.619 * (x^{+})^{-\frac{1}{3}} \tag{6.4}$$

Heat transfer calculated for the entrance domain is then derived from equation 6.4 to be:

$$h = (k^{2} * \rho * c)^{\frac{1}{3}} \tag{6.5}$$

From this, the heat transfer ratios obtained from measurements and predictions are compared for a range of volume fractions

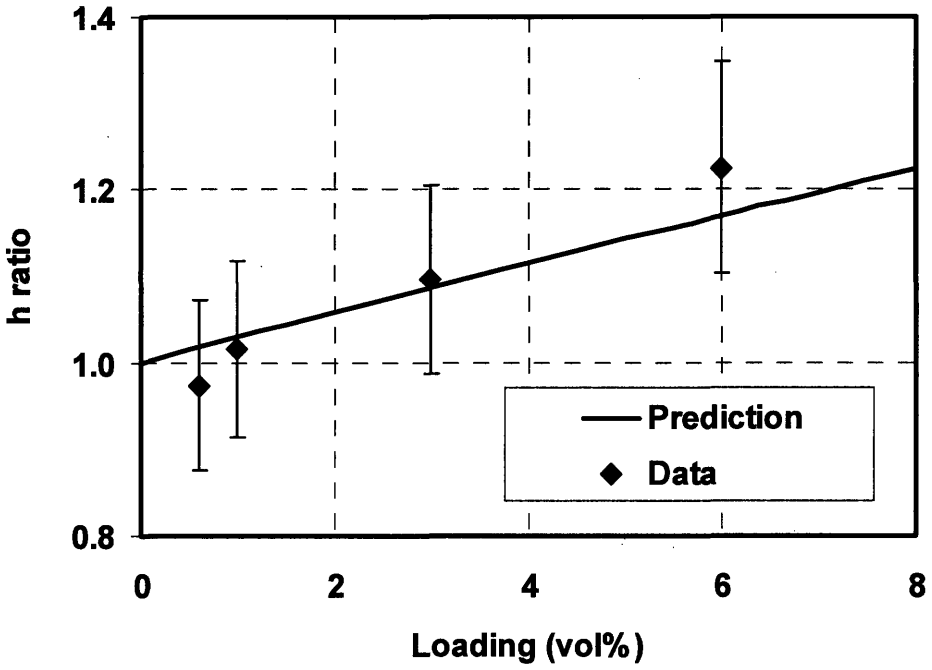


**Figure 6.10: The above graph is the heat transfer coefficient ratio found in the entrance region**

At 6 vol% of Alumina, there is 21% heat transfer enhancement compared to the expected value of 17%. The above graph displays no abnormal enhancement that is found from the entrance region beyond what is predicted by using the correct properties of alumina.

## 6.3 ZIRCONIA TESTS

The Zirconia runs consisted of 20 experimental runs at 7, 3.5, and 1.7 weight percent. Similar procedures were taken to verify that the experimental loop was still operating at optimal conditions. Pressure was taken with the results to understand if there was error that could be found with the system. During experimentation, it was observed that steady-state time took significantly longer to maintain with zirconia, than with alumina. Steady-state was reached approximately 30 to 45 minutes for the runs. This steady-state time decreased with increasing dilution weight percent of the zirconia. This

led to a fewer number of runs completed due to the excessive time commitment. The below graph was found:

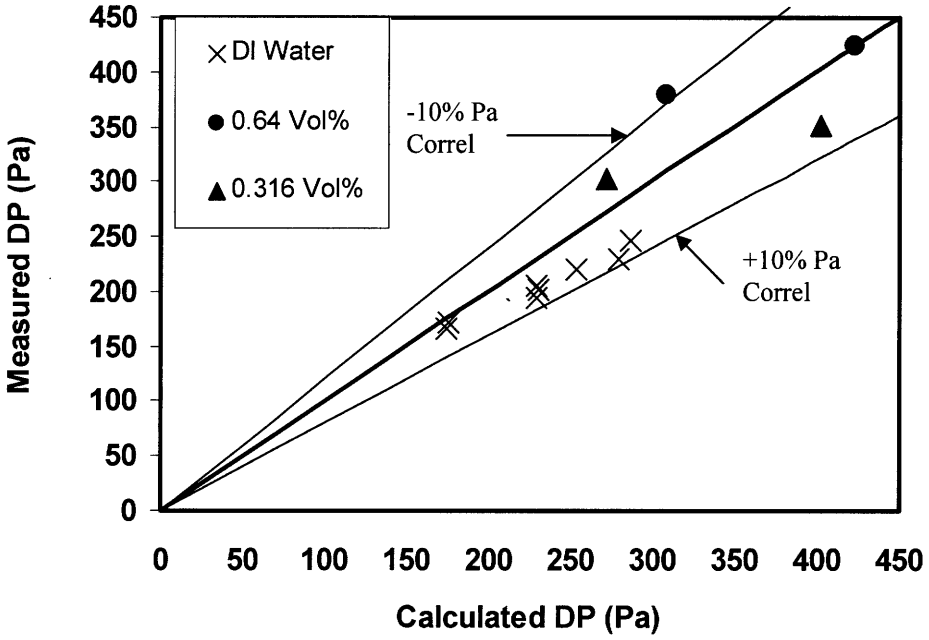


**Figure 6.11: Compares DI water and Zirconia with measured and calculated pressure values.**

The results display no known differences that can be found in the apparatus. Thus, the experimental runs began starting with 7 weight percent of zirconia.

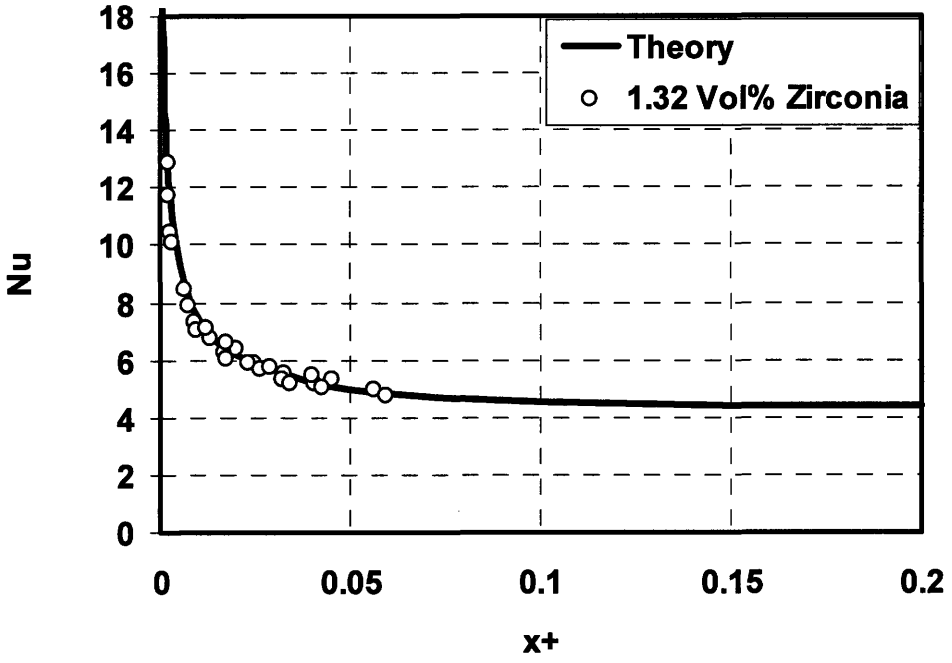


**Figure 6.12: 7 weight percent Nusselt number versus axial location**

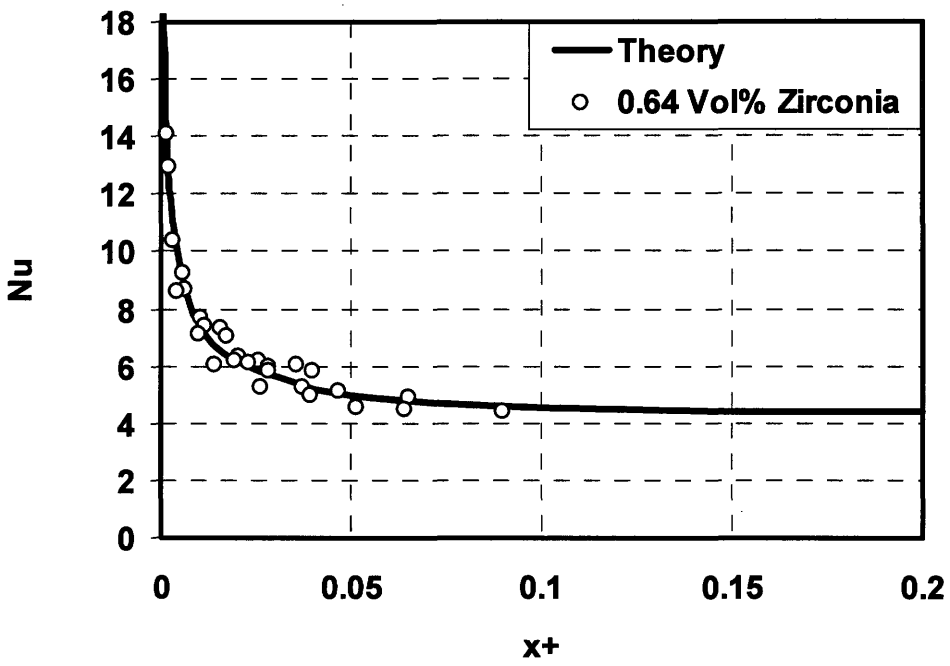


**Figure 6.13: Calculated zirconia values of Nusselt number and its axial location plotted against theory**

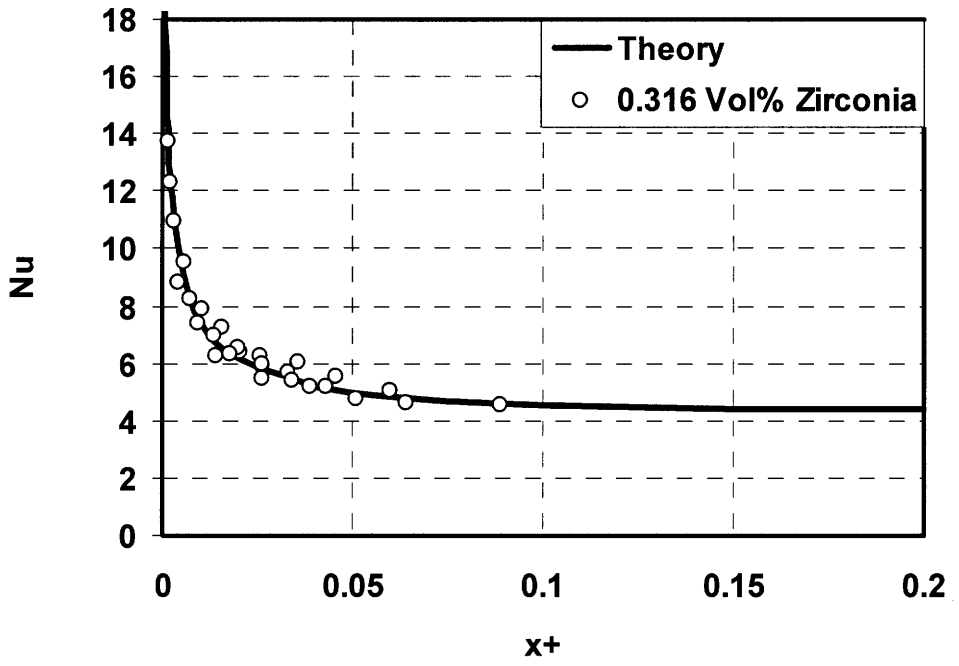


**Figure 6.14: Compares the Nusselt number with axial location at 1.7 weight percent zirconia**

The trend that is found from the figures above shows no heat enhancement effect. All the experimental data taken and plotted fit the theoretical curve. These results are similar to that of the alumina results found earlier.

# CHAPTER 7

# CONCLUSION

The purpose of this study was to observe and measure heat transfer rate and viscous pressure loss of alumina and zirconia nanofluids in laminar flow regime. A vertical flow loop was designed and constructed for this work. The heated section is 4.5 mm in ID and 1.0 m in length with thermocouples installed on the outer wall axially. .Pressure drop was measured in an isothermal section of the loop. Validation tests were performed for de-ionized water to ensure the loop operates as expected.

The heat transfer coefficient data taken for zirconia and alumina, represented in dimensionless Nusselt number and distance, were found to fit the predictions, as long as the measured mixture thermal conductivity and viscosity are used. The measured viscous pressure drop was found to be within 20% of theory. It is concluded that with the proper properties used there is no abnormal heat transfer or viscous pressure loss associated with the use of nanofluids in laminar flow. That is, as long as the accurate nanofluid properties are used, the heat transfer coefficient and pressure drop for laminar flow can be predicted with existing models. In conclusion, no irregular heat enhancement was found in convective heat transfer in the laminar flow regime.

# APPENDIX A

# TABLE OF EXPERIMENTAL DATA

Note: Experiments noted with asterisks are not used in final data analysis because of Re>2000 or heat loss > 11%

Table A.1: DI Water results

| Experiment (Name #) | Vol % | Flow rate (gpm) | $Temp_{inlet}$ (C) | $Temp_{outlet}$ (C) | Heat Loss | Re |
|---|---|---|---|---|---|---|
| DI #1 | 0% | 0.049 | 26.50 | 36.71 | 10.70% | 1035.39 |
| DI #2 | 0% | 0.048 | 21.81 | 30.49 | 4.88% | 936.56 |
| DI #3 | 0% | 0.049 | 21.78 | 32.53 | 5.27% | 976.10 |
| DI #4 | 0% | 0.040 | 22.05 | 30.98 | 8.50% | 780.14 |
| DI #5 | 0% | 0.040 | 21.84 | 31.46 | 7.86% | 779.89 |
| DI #6 | 0% | 0.039 | 21.89 | 31.56 | 8.08% | 774.52 |
| *DI #7 | 0% | 0.030 | 22.03 | 31.90 | 13.20% | 601.20 |
| *DI #8 | 0% | 0.030 | 21.89 | 32.33 | 13.72% | 594.51 |
| *DI #9 | 0% | 0.028 | 21.83 | 31.87 | 14.84% | 561.80 |
| *DI #10 | 0% | 0.019 | 22.25 | 31.12 | 23.18% | 386.15 |
| *DI #11 | 0% | 0.020 | 21.92 | 30.23 | 23.60% | 392.11 |
| *DI #12 | 0% | 0.019 | 21.81 | 31.44 | 25.34% | 382.33 |

Table A.2: Alumina 19.5 wt% Results

| 19.50 Weight % | Vol % | Flow rate (gpm) | $Temp_{inlet}$ (C) | $Temp_{outlet}$ (C) | Heat Loss | Re |
|---|---|---|---|---|---|---|
| ALR #1 | 6% | 0.251 | 25.62 | 34.84 | 2.43% | 1089.36 |
| ALR #2 | 6% | 0.252 | 26.21 | 36.20 | 2.13% | 1117.04 |
| ALR #3 | 6% | 0.205 | 25.66 | 34.54 | 3.33% | 803.39 |
| ALR #4 | 6% | 0.203 | 25.74 | 35.68 | 2.43% | 891.39 |
| ALR #5 | 6% | 0.150 | 25.23 | 34.30 | 6.56% | 644.13 |
| ALR #6 | 6% | 0.150 | 25.60 | 35.77 | 6.68% | 552.44 |
| ALR #7 | 6% | 0.103 | 24.21 | 33.36 | 10.73% | 430.95 |
| *ALR #8 | 6% | 0.101 | 24.32 | 34.78 | 11.43% | 431.80 |
| *ALR #9 | 6% | 0.051 | 22.90 | 33.04 | 19.56% | 209.55 |
| *ALR #10 | 6% | 0.051 | 22.38 | 31.86 | 18.06% | 205.45 |
| *ALR #11 | 6% | 0.039 | 22.42 | 32.75 | 22.99% | 158.91 |
| *ALR #12 | 6% | 0.030 | 22.05 | 32.56 | 28.00% | 121.52 |
| *ALR #13 | 6% | 0.022 | 22.33 | 31.13 | 29.18% | 87.69 |
| *ALR #14 | 6% | 0.019 | 22.26 | 33.26 | 35.42% | 80.47 |

Table A.3: Alumina 10.8 wt% Results

| 10.80 Weight % | Vol % | Flow rate (gpm) | $Temp_{inlet}$ (C) | $Temp_{outlet}$ (C) | Heat Loss | Re |
|---|---|---|---|---|---|---|
| *ALR #15 | 3% | 0.201 | 24.58 | 33.81 | -0.92% | 2301.65 |
| ALR #16 | 3% | 0.151 | 23.07 | 32.41 | 1.15% | 1666.05 |
| ALR #17 | 3% | 0.102 | 22.93 | 33.15 | 2.85% | 1130.83 |
| ALR #18 | 3% | 0.090 | 22.74 | 32.58 | 3.27% | 992.08 |
| ALR #19 | 3% | 0.089 | 22.27 | 30.88 | 3.10% | 957.49 |
| ALR #20 | 3% | 0.087 | 22.13 | 30.91 | 3.92% | 930.29 |
| ALR #21 | 3% | 0.052 | 21.38 | 31.78 | 8.11% | 561.76 |
| ALR #22 | 3% | 0.050 | 21.57 | 31.71 | 9.89% | 535.17 |
| *ALR #23 | 3% | 0.039 | 21.98 | 32.90 | 13.29% | 431.00 |
| *ALR #24 | 3% | 0.039 | 21.65 | 32.03 | 13.29% | 428.21 |
| *ALR #25 | 3% | 0.029 | 21.95 | 32.37 | 17.82% | 319.37 |
| *ALR #26 | 3% | 0.030 | 21.72 | 31.45 | 16.72% | 326.52 |
| *ALR #27 | 3% | 0.020 | 22.33 | 33.13 | 22.81% | 224.48 |
| *ALR #28 | 3% | 0.019 | 22.18 | 32.78 | 23.20% | 216.90 |

Table A.4: Alumina 4.44 wt% Results

| 4.44 Weight % | Vol% | Flow rate (gpm) | $Temp_{inlet}$ (C) | $Temp_{outlet}$ (C) | Heat Loss | Re |
|---|---|---|---|---|---|---|
| *ALR #29 | 1% | 0.149 | 22.44 | 31.43 | 1.73% | 2586.82 |
| ALR #30 | 1% | 0.108 | 22.62 | 31.83 | 2.21% | 1888.19 |
| ALR #31 | 1% | 0.050 | 21.73 | 31.27 | 5.19% | 870.19 |
| ALR #32 | 1% | 0.049 | 21.55 | 32.02 | 6.64% | 857.89 |
| ALR #33 | 1% | 0.050 | 21.48 | 31.38 | 6.78% | 852.19 |
| ALR #34 | 1% | 0.039 | 21.73 | 32.63 | 10.53% | 684.90 |
| ALR #35 | 1% | 0.041 | 21.57 | 31.81 | 7.20% | 718.93 |
| ALR #36 | 1% | 0.038 | 21.61 | 31.76 | 10.09% | 666.74 |
| *ALR #37 | 1% | 0.029 | 20.84 | 32.08 | 15.48% | 505.24 |
| *ALR #38 | 1% | 0.029 | 21.18 | 31.57 | 13.68% | 504.38 |
| ALR #39 | 1% | 0.032 | 21.49 | 30.58 | 10.13% | 551.01 |
| *ALR #40 | 1% | 0.022 | 22.23 | 31.54 | 17.76% | 386.73 |
| *ALR #41 | 1% | 0.022 | 22.19 | 31.83 | 16.89% | 387.74 |
| *ALR #42 | 1% | 0.019 | 22.29 | 32.62 | 20.89% | 343.67 |

Table A.5: Alumina 2.16 wt% Results

| 2.16 Weight % | Vol % | Flow rate (gpm) | $Temp_{inlet}$ (C) | $Temp_{outlet}$ (C) | Heat Loss | Re |
|---|---|---|---|---|---|---|
| ALR #43 | 0.01% | 0.101 | 21.72 | 31.98 | -0.67% | 1797.14 |
| ALR #44 | 0.01% | 0.102 | 20.59 | 30.51 | 3.74% | 1762.12 |
| ALR #45 | 0.01% | 0.050 | 21.40 | 30.99 | 4.72% | 883.81 |
| ALR #46 | 0.01% | 0.052 | 21.27 | 30.53 | 4.07% | 907.01 |
| ALR #47 | 0.01% | 0.050 | 21.32 | 31.14 | 4.97% | 881.14 |
| ALR #48 | 0.01% | 0.040 | 21.51 | 31.35 | 6.90% | 707.61 |
| ALR #49 | 0.01% | 0.042 | 21.37 | 30.68 | 5.52% | 738.19 |
| ALR #50 | 0.01% | 0.040 | 21.36 | 30.80 | 6.11% | 710.39 |
| *ALR #51 | 0.01% | 0.029 | 21.69 | 32.72 | 11.54% | 532.41 |
| *ALR #52 | 0.01% | 0.028 | 21.64 | 32.12 | 12.16% | 509.20 |
| *ALR #53 | 0.01% | 0.019 | 22.07 | 31.68 | 18.90% | 353.83 |
| *ALR #54 | 0.01% | 0.021 | 21.75 | 31.55 | 18.97% | 383.44 |

Table A.6: Zirconia 7 wt% Results

| 7 Weight % | Vol % | Flow rate (gpm) | $Temp_{inlet}$ (C) | $Temp_{outlet}$ (C) | Heat Loss | Re |
|---|---|---|---|---|---|---|
| ZR #1 | 1.32% | 0.079 | 22.08 | 33.63 | 7.09% | 1204.29 |
| ZR #2 | 1.32% | 0.063 | 22.09 | 31.89 | 5.71% | 959.67 |
| ZR #3 | 1.32% | 0.060 | 21.48 | 31.92 | 7.63% | 900.55 |
| ZR #4 | 1.32% | 0.089 | 22.01 | 34.26 | 5.85% | 1366.56 |
| *ZR #5 | 1.32% | 0.023 | 21.78 | 35.78 | 26.71% | 366.13 |
| *ZR #6 | 1.32% | 0.034 | 21.21 | 36.78 | 18.04% | 530.77 |

TableA.7: Zirconia 3.5 wt% Results

| 3.5 Weight % | Vol % | Flow rate (gpm) | $Temp_{inlet}$ (C) | $Temp_{outlet}$ (C) | Heat Loss | Re |
|---|---|---|---|---|---|---|
| ZR #7 | 0.64% | 0.101 | 20.93 | 34.32 | 6.77% | 1417.79 |
| ZR #8 | 0.64% | 0.090 | 22.28 | 32.79 | 5.63% | 1263.17 |
| ZR #9 | 0.64% | 0.055 | 21.75 | 35.56 | 8.12% | 786.85 |
| ZR #10 | 0.64% | 0.040 | 21.15 | 32.46 | 13.36% | 555.15 |
| *ZR #11 | 0.64% | 0.027 | 20.98 | 32.85 | 20.38% | 375.71 |
| *ZR #12 | 0.64% | 0.018 | 20.86 | 32.28 | 31.35% | 258.61 |
| *ZR #13 | 0.64% | 0.218 | 22.92 | 32.80 | 1.29% | 3056.24 |

Table A.8 Zirconia 1.75 wt% Results

| 1.75 Weight % | Vol % | Flow rate (gpm) | $Temp_{inlet}$ (C) | $Temp_{outlet}$ (C) | Heat Loss | Re |
|---|---|---|---|---|---|---|
| *ZR #14 | 0.32% | 0.228 | 21.81 | 31.63 | 1.76% | 3612.23 |
| ZR #15 | 0.32% | 0.102 | 22.04 | 32.62 | 4.36% | 1626.74 |
| ZR #16 | 0.32% | 0.079 | 21.96 | 32.87 | 5.79% | 1269.59 |
| ZR #17 | 0.32% | 0.061 | 21.73 | 33.22 | 7.59% | 974.26 |
| ZR #18 | 0.32% | 0.040 | 21.05 | 32.06 | 10.15% | 644.10 |
| *ZR #19 | 0.32% | 0.032 | 20.80 | 30.66 | 14.51% | 499.39 |
| *ZR #20 | 0.32% | 0.020 | 20.76 | 31.24 | 29.83% | 324.88 |

## BIBLIOGRAPHY

[1] Stephen U.S. Choi,"Nanofluid Technology: Current Status and Future Research, Energy Technology Division Argonne National Laboratory, Argonne, IL September 1999

[2] Mike Garvey, "The Impact of Colloid Science" Chemistry World, February (2003)

[3] Seok Pil Jang and Stephen U.S. Choi, "Role of Brownian motion in the Enhanced Thermal Conductivity of Nanofluids" Applied Physics Letter May (2004)

[4] Kiyeul Kwak and Chongyoup Kim, "Viscosity and Thermal Conductivity of Copper Oxide Nanofluid Dispersed in Ethylene Glycol" Dept. of Chemical and Biological Engineering, Korea University, April (2005)

[5] Yimin Xuan and Qiang Li, "Investigation on Convective Heat transfer and Flow Features of Nanofluids" Journal of Heat Transfer, Copyright 2005 Elsevier Engineering Information Inc.

[6] Wesley Charles Williams, "Experimental and Theoretical Investigation of Transport Phenomena in Nanoparticle Colloids (Nanofluids)", Department of Nuclear Science and Engineer at Massachusetts Institute of Technology, December (2006)

[7] DongSheng Wen and Yulong Ding, "Experimental investigation into convective heat transfer of nanofluids at the entrance region under laminar flow conditions" International Journal of Heat and Mass Transfer September (2004)

[8] Avtar Aingh Ahuja, "Augmentations of heat transport in laminar flow of polystyrene suspensions", Journal of Applied Physics August (1975)

[9] Jacopo Buongiorno "Convective Transport in Nanofluids" Transactions of the ASME March (2006)

[10] Nyacol Nanotechnology, http://www.nyacol.com/A120PQ3-99.htm, (2007).

[11] Sung Joong Kim, "Pool Boiling Heat Transfer Characteristics of Nanofluids", Department of Nuclear Science and Engineer at Massachusetts Institute of Technology, May (2007)

[12] Shigeki Yatsuya, Takayoshi Hayashi, Hiroshi Akoh, Eiji Nakamura, Akira Tasaki, "Magnetic Properties of Extremely Fine Particles of Iron Prepared by Vacuum Evaporation on Running Oil Substrate", Japanese Journal of Applied Physics February (1978)

[13] Traci Bradford and M. Nicole Cook, "Inductively Coupled Plasma" http://www.cee.vt.edu/ewr/environmental/teach/smprimer/icp/icp.html December 1997

[14] Fox, Robert and McDonald, Alan "Introduction to Fluid Mechanics" John Wily & Sons, Inc. New York pp 38-41

[15] Kays, William and Crawford, Michael "Convective Heat and Mass Transfer" McGraw-Hill Science Engineering pp 103-14

[16] Omega Engineering, http://www.omega.com/thermocouples.html, (2007).

[17] J. H Lienhard IV and J. H. Lienhard V, A Heat Transfer Textbook, 3rd edition, Phlogiston Press, 2002

[18] J. F. Douglas, M. J. Gasiorek, J. A. Swaffield , Fluid Mechanics, Longman Publishers, 1994

[19] Omega Engineering, http://www.omega.com/prodinfo/pressuretransducers.html, (2007).